










# A NEW SMALL, MESOROSTRINE INIOID (CETACEA, ODONTOCETI, DELPHINIDA) FROM FOUR UPPER MIOCENE LOCALITIES IN THE PISCO BASIN, PERU

by OLIVIER LAMBERT<sup>1</sup> , ALBERTO COLLARETA<sup>2</sup> ,  
ALDO BENITES-PALOMINO<sup>3,4</sup> , CLAUDIO DI CELMA<sup>5</sup> ,  
CHRISTIAN DE MUIZON<sup>6</sup> , MARIO URBINA<sup>4</sup>  and  
GIOVANNI BIANUCCI<sup>2</sup> 

<sup>1</sup>Direction Opérationnelle Terre et Histoire de la Vie, Institut Royal des Sciences Naturelles de Belgique, rue Vautier 29, 1000, Brussels, Belgium; olambert@naturalsciences.be

<sup>2</sup>Dipartimento di Scienze della Terra, Università di Pisa, Via S. Maria 53, 56126, Pisa, Italy

<sup>3</sup>Paläontologisches Institut und Museum, Universität Zürich, Karl-Schmid-Straße 4, 8006, Zürich, Switzerland

<sup>4</sup>Departamento de Paleontología de Vertebrados, Museo de Historia Natural – UNMSM, Avenida Arenales 1256, 15072, Lima, Peru

<sup>5</sup>Scuola di Scienze e Tecnologia, Università di Camerino, Via Gentile III da Varano 1, 62032, Camerino, Italy

<sup>6</sup>Département Origines et Evolution, CR2P UMR 7207, (MNHN, CNRS, UPMC, Sorbonne-Université), Muséum national d'Histoire naturelle, rue Cuvier 57, 75231, Paris, France

Typescript received 25 March 2020; accepted in revised form 22 May 2020

**Abstract:** The moderately rich past diversity of the superfamily Iniioidea (Cetacea, Odontoceti) in both the Atlantic and Pacific oceans contrasts with the present survival of a single genus (*Inia*, Amazon river dolphin, family Iniidae) in freshwater deposits of South America and of a single species (*Pontoporia blainvillei*, franciscana, family Pontoporiidae) along the eastern coast of that continent. However, part of the late Miocene – Pliocene inioid fossil record consists of relatively fragmentarily known species, for which systematic affinities remain poorly understood. Based on a sample of six cranial specimens from lower upper Miocene (Tortonian, 9.5–8.6 Ma) marine deposits of the Pisco Formation exposed at four localities of the East Pisco Basin (southern coast of Peru), we describe a new genus and species of inioid, *Samydelphis chacaltanae*. This mesorostrine, small-sized species is characterized by an upper tooth count of *c.* 30 teeth per

row, a moderately elevated vertex of the cranium displaying a long anteromedial projection of the frontals and interparietal, and the plesiomorphic retention of a premaxilla–nasal contact. Recovered as a member of the family Pontoporiidae in our phylogenetic analysis, *S. chacaltanae* falls as sister group to *Meherrinia isoni*, from the upper Miocene of North Carolina (USA), which has previously been tentatively referred to the Iniidae or regarded as a stem Iniioidea. Originating from the P1 allomember of the Pisco Formation, the mesorostrine *S. chacaltanae* was contemporaneous and sympatric with two other inioids, the brevirostrine pontoporiid *Brachydelphis mazeasi* and the longirostrine iniid *Brujadelphis ankylorostris*.

**Key words:** Iniioidea, Pontoporiidae, dolphin, late Miocene, Tortonian, Pisco Formation.

THE two modern inioid (Cetacea, Odontoceti, Iniioidea) genera, *Inia* (the Amazon river dolphin, the only extant member of the family Iniidae; Best & da Silva 1989) and *Pontoporia* (the franciscana, the only extant member of the family Pontoporiidae, from the coastal ecosystems along the eastern coast of South America; Brownell 1989), represent relics of a once much more diversified toothed cetacean clade (Cozzuol 2010; Marx *et al.* 2016). With a fossil record traced back to the late Miocene, extinct inioids have been recorded from numerous marine and, to a lesser extent, freshwater deposits around the world, testifying to a

much broader past geographical distribution that spanned the north and south-east Atlantic as well as the north-western and south-eastern Pacific (Pyenson & Hoch 2007; Godfrey & Barnes 2008; Gibson & Geisler 2009; Geisler *et al.* 2012; Pyenson *et al.* 2015; Murakami 2016; Post *et al.* 2017; Lambert *et al.* 2018). The prevalence of extinct inioids in marine deposits and their broad geographic distribution have been used as arguments in favour of the hypothesis of an ancestral habitat in marine environments for these small to medium-sized dolphins (Cassens *et al.* 2000; Hamilton *et al.* 2001; Geisler *et al.* 2011).

The past diversity of this clade in South America can be divided into two geographical and palaeoenvironmental domains: on the one hand, the freshwater deposits of Brazil and Argentina; on the other hand, the marine deposits along the Atlantic, Caribbean, and Pacific coasts of the continent (Muizon 1984, 1988a; Gutstein *et al.* 2009, 2014; Cozzuol 2010; Lambert & Muizon 2013; Aguirre-Fernández *et al.* 2017; Lambert *et al.* 2017). A vast majority of the late Miocene marine records originate from the East Pisco and Sacaco basins, which are located along the southern coast of Peru and are famous for their extremely rich and increasingly well-stratigraphically constrained marine mammal assemblages (e.g. Muizon 1984, 1988a; Bianucci *et al.* 2016a, b; Bosio *et al.* 2020a, b). Furthermore, the degree of completeness of inioid cranial remains from these two nearby regions contrasts markedly with fossil inioid material from other parts of the world. For example, finely preserved iniid and pontoporiid remains from the East Pisco Basin provided useful clues on the anatomy of cranial parts (e.g. the highly diagnostic ear bones) that are not preserved in closely related taxa from Central America and the North Atlantic (Lambert & Muizon 2013; Lambert *et al.* 2017). Further exploiting this unique source of information on the early steps of the inioid evolutionary history, based on six new cranial specimens, mandible fragments, and a few associated vertebrae from early late Miocene deposits exposed at four localities of the East Pisco Basin (Fig. 1), herein we describe a new inioid genus and species, and we investigate its phylogenetic relationships with other inioids worldwide.

## GEOLOGICAL, STRATIGRAPHIC AND PALAEOLOGICAL FRAMEWORK

The East Pisco shelf basin in southern Peru is an extensional forearc basin elongated parallel to the Peruvian trench and is separated from the adjacent West Pisco upper-slope basin by a structural high (the Outer Shelf High), which is composed of Precambrian and Palaeozoic metamorphic and igneous rocks (Thornburg & Kulm 1981; León *et al.* 2008). During much of its Cenozoic depositional history, the East Pisco Basin was a semi-enclosed, shallow-water, marine embayment protected seawards by a chain of basement islands (Marocco & Muizon 1988; Bianucci *et al.* 2018). Following rapid uplift during the latest Neogene (Pilger 1981; Hsu 1992; Macharé & Ortlieb 1992; Hampel *et al.* 2004), the basin fill became largely exposed in the present-day Ica Region, between the towns of Pisco and Nazca.

The sediments from which the fossil cetaceans described herein were collected are part of the middle–upper Miocene strata of the Pisco Formation exposed in the Ica desert. The Pisco Formation is the geologically youngest unit among

those comprising the sedimentary fill of the East Pisco Basin (Dunbar *et al.* 1990; DeVries 1998), and consists of shallow-marine and offshore deposits (including gravels, sandstones, diatomaceous siltstones, nodular dolomitic beds, and tephra layers) that are believed to reflect pronounced coastal upwelling and high primary productivity conditions (Suess *et al.* 1988; Dunbar *et al.* 1990; Brand *et al.* 2004). Along the western bank of the Ica River, south and west of the Ocucaje village, two basin-wide erosional surfaces cut the Pisco strata, each reflecting a period of subaerial exposure and, as such, a break in the sedimentary history of the basin (Di Celma *et al.* 2017, 2018). Consequently, the Pisco Formation can be divided into three unconformity-bounded stratal packages (i.e. allomembers), designated P0, P1, and P2 in ascending stratigraphic order, which progressively onlap north-eastwards a composite basal unconformity; each allomember consists of a coarse-grained lower portion, mostly comprising nearshore gravels and sandstones, that passes upwards into an offshore interval of diatomaceous mudstones (Di Celma *et al.* 2017, 2018; DeVries & Jud 2018). The depositional age of the three Pisco allomembers in the study area has been recently constrained by means of diatom biostratigraphy, Ar–Ar radiochronology, and strontium isotope stratigraphy (Gariboldi *et al.* 2017; Bosio *et al.* 2019, 2020a, b): thus, P0 was deposited *c.* 14.8–12.4 Ma (i.e. during the Langhian–Serravallian), P1 *c.* 9.5–8.6 Ma (i.e. during the Tortonian), and P2 *c.* 8.4–6.7 Ma (i.e. during the Tortonian–Messinian). These age estimates suggest that, at least in part, the deposition of the Pisco allomembers was controlled by glacio-eustatic fluctuations in sea level (Di Celma *et al.* 2018).

All the specimens of the new inioid species described herein for which the stratigraphic whereabouts are known come from beds pertaining to the P1 allomember (referred to as the ‘Cerro Colorado lower allomember’ by Di Celma *et al.* 2016). In particular, five stratigraphically framed finds are known from P1 exposures at the sites of Cerro Colorado (MUSM 565, MUSM 566, and MUSM 2541), south of Cerro la Bruja (MUSM 3902), and a locality informally named ‘Anfiteatro’ by Bosio *et al.* (2020b) located between Cerro los Quesos and Cerros Cadena de los Zanjones (MUSM 3903); a sixth specimen, MUSM 2512, comes from undifferentiated Pisco strata cropping out at the locality known as Corre Viento (a broad outcrop area, characterized by exposures of both the P1 and P2 allomembers, whose stratigraphic asset is nonetheless still largely unknown; Fig. 2). The P1 stratal package exhibits its maximum thickness (*c.* 100 m) in its southern exposures, in the vicinities of Cerros Cadena de los Zanjones and Cerros la Mama y la Hija, where they rest unconformably on P0 deposits (Di Celma *et al.* 2017, 2018). Towards the northeast, P1 thins significantly to become *c.* 40 m thick at Cerro la Bruja, beyond which it is thought to disappear as a result of progressive north-

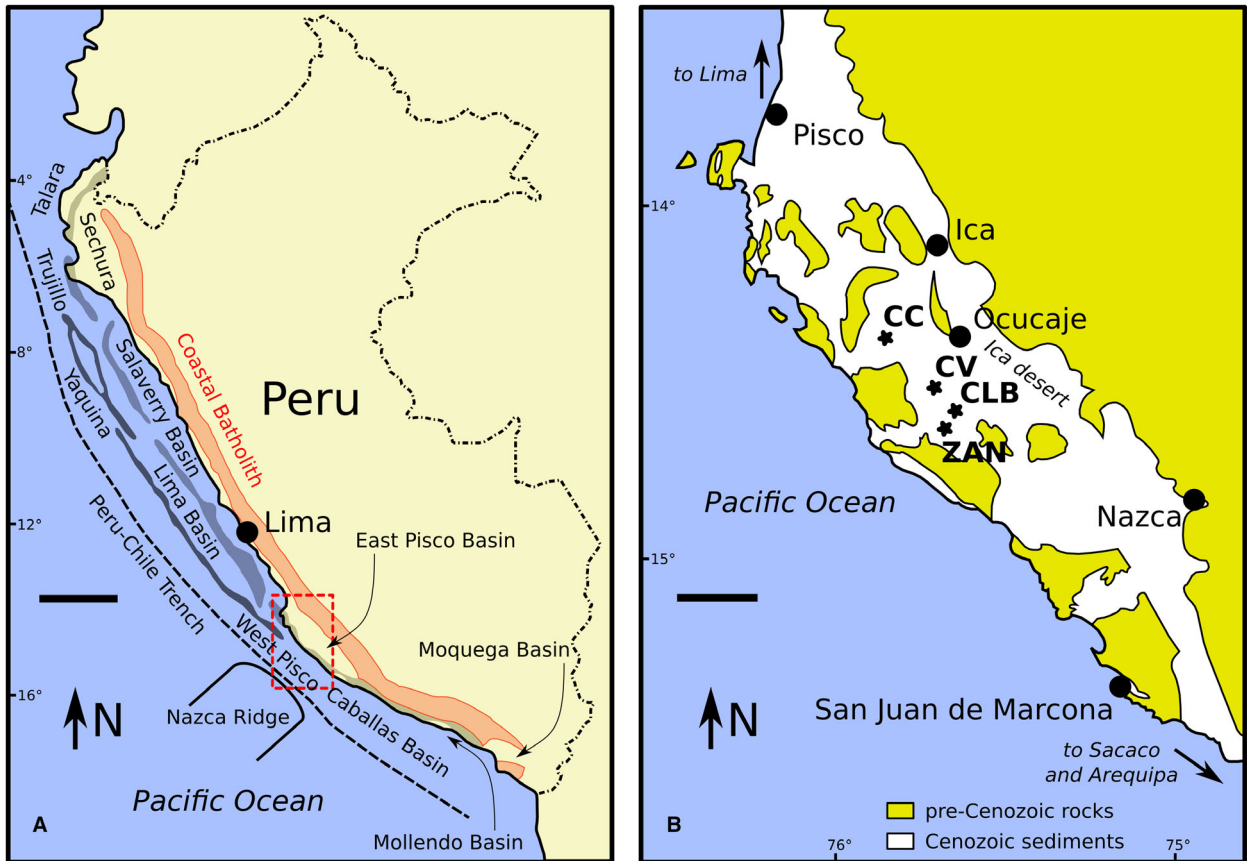


**FIG. 1.** A, sketch map of the major structural trends and basins of coastal Peru. The red dashed rectangle indicates the location of the East Pisco Basin, shown in detail in B; redrawn and modified from Travis *et al.* (1976) and Thornburg & Kulm (1981).

B, schematic geological map of the East Pisco Basin, showing the areas of outcrop of the Cenozoic basin fill and the location of the sites (black stars) where the holotype and referred specimens of the new inioid taxon *Samaydelphis chacaltanae* described herein were found; redrawn and modified from DeVries & Schrader (1997). *Abbreviations:* CC, Cerro Colorado; CLB, Cerro la Bruja; CV, Corre Viento; ZAN, Cerros Cadena de los Zanjones. Scale bars represent: 200 km (A); 25 km (B).

eastward onlap onto the basin basement (Di Celma *et al.* 2017). Some 30 km to the northwest of Cerro la Bruja, at Cerro Colorado, P1 is *c.* 75 m thick, its lower boundary consisting of an angular unconformity with the underlying strata of the Chilcatay Formation (Di Celma *et al.* 2016).

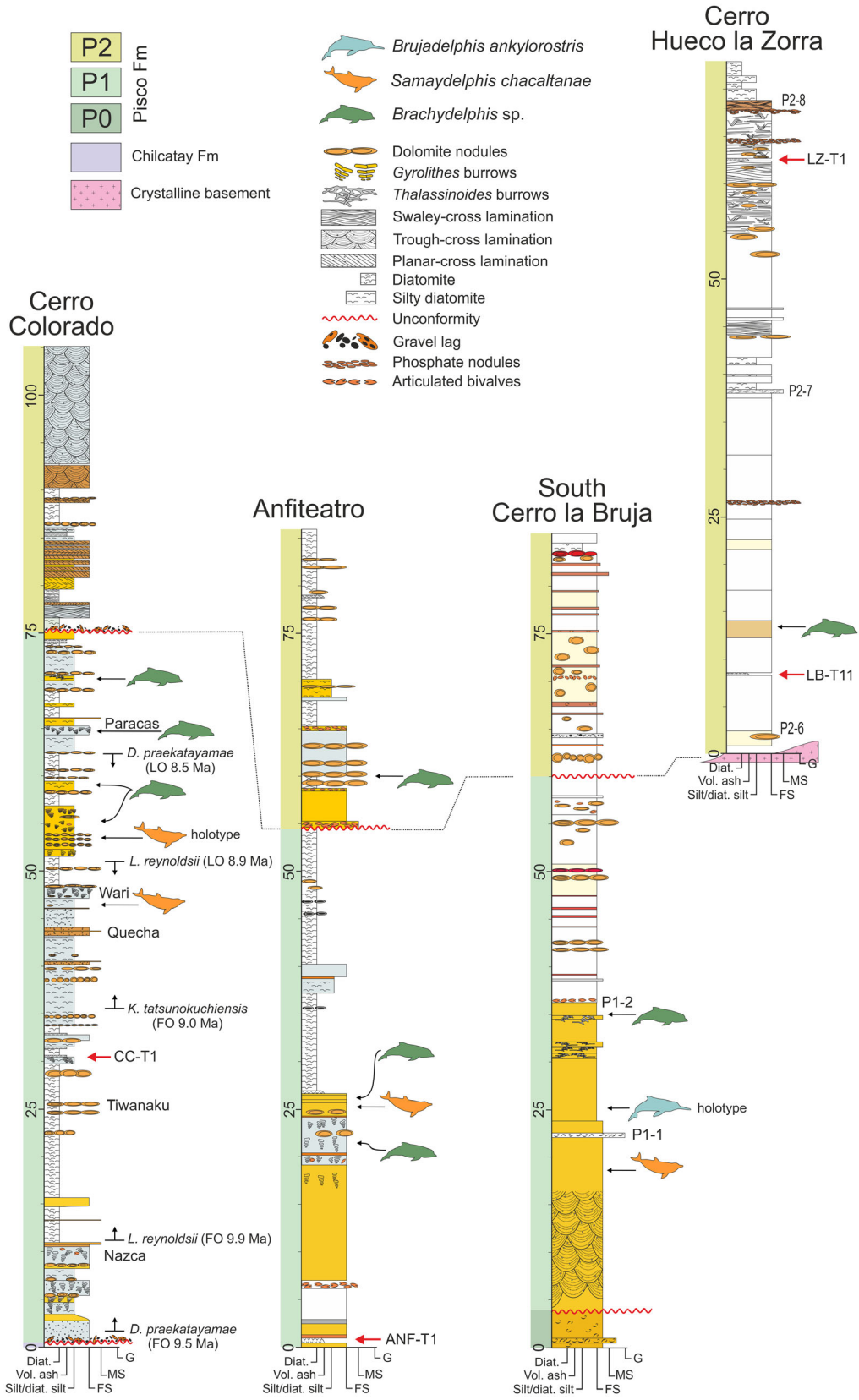
The P1 allomember features a copious, diverse, and well-preserved fossil vertebrate assemblage that consists of cetaceans (including both mysticetes and odontocetes), pinnipeds, bony and cartilaginous fishes (including both sharks and rays), seabirds, crocodylians, and marine turtles (Parham & Pyenson 2010; Bianucci *et al.* 2010; Lambert *et al.* 2009, 2010; Bianucci *et al.* 2016a, b; Stucchi *et al.* 2016; Landini *et al.* 2017a, 2017b; Ramassamy *et al.* 2018). Fossils of cetaceans are particularly numerous, the remains of baleen-bearing whales (consisting of a large-sized cetotheriid species and 2–3 balaenopterid species) being more abundant, but less diverse, than those of toothed whales (represented by two ziphiids, *Chimuziphius coloradensis* and *Messapicetus gregarius*, two

physeteroids, *Livyatan melvillei* and *Acrophyseter* sp., two or more undescribed kentriodontid-like delphinidans, the pontoporiid inioid *Brachydelphis mazeasi*, the inioid *Brujadelphis ankylorostris*, and the new inioid taxon described herein). Cases of exceptional preservation from the deposits referred to the P1 allomember include the fossilized digestive tract contents of two cetaceans (a cetotheriid and a specimen of *Messapicetus gregarius*), revealing predation upon pilchards, and the phosphatized baleen of a balaenopterid whale (Collareta *et al.* 2015; Lambert *et al.* 2015; Gioncada *et al.* 2016).

## MATERIAL AND METHOD

### Anatomical terminology

Terminology for skull anatomy follows Mead & Fordyce (2009), unless otherwise stated.



### Phylogeny

To investigate its phylogenetic relationships, the new taxon was coded in the character–taxon matrix of Lambert *et al.* (2018), modified from Geisler *et al.* (2011, 2012), Lambert *et al.* (2017), and Post *et al.* (2017), resulting in a matrix of 109 taxa and 324 characters (for the character–taxon matrix, see Lambert *et al.* 2020, file 1). As in previous analyses based on this matrix, we used Paup 4.0 (Swofford 2003); three outgroups (*Bos taurus*, *Hippopotamus amphibius*, and *Sus scrofa*) were defined; and ordered multistate characters were scaled for a minimum length of each being one step. Slightly differing from previous analyses, the constraint tree enforced as a backbone results from more recent maximum likelihood and Bayesian analyses of a very large genomic dataset on extant species (McGowen *et al.* 2019; Lambert *et al.* 2020, file 2). Most parsimonious trees were obtained by heuristic search, using the tree-bisection-reconnection branch-swapping algorithm and the ACCTRAN character-state optimization. Bootstrap values were calculated with Paup 4.0 (100 replicates).

*Institutional abbreviation.* MUSM, Museo de Historia Natural, Universidad Nacional Mayor de San Marco, Lima, Peru.

## SYSTEMATIC PALAEOLOGY

Order CETACEA Brisson, 1762

PELAGICETI Uhen, 2008

NEOCETI Fordyce & Muizon, 2001

Suborder ODONTOCETI Flower, 1867

Infraorder DELPHINIDA Muizon, 1984

Superfamily INIOIDEA Muizon, 1988b

Family PONTOPORIIDAE Kasuya, 1973

*Remarks.* The new genus and species described herein is attributed to the family Pontoporiidae (defined as the clade grouping all the inioids more closely related to *Pontoporia* than to *Inia*), mostly based on the results of the phylogenetic analysis and one morphological feature, the anteroposterior elongation of the nasals typical for pontoporiids (Muizon 1984, 1988a). However, the support for this clade remains relatively low (see Discussion below), and the topology of this part of the odontocete tree may change with the addition of taxa based on more complete specimens. More specifically, the discovery of new specimens for the

new genus and species described herein (based on six cranial specimens), including the highly informative, but unfortunately easily detached ear bones (especially the periotic), may confirm its attribution to the Pontoporiidae (Muizon 1984, 1988a).

### Genus SAMAYDELPHIS nov.

*LSID.* urn:lsid:zoobank.org:act:D36013AD-EBE7-4A19-8559-C36FAA95E7A8

*Derivation of name.* From *samay*, ‘intermediate’ in Quechua, referring to the cranial morphology of the new taxon being intermediate between the iniid *Inia* and the pontoporiid *Pontoporia*; and from *delphis*, ‘dolphin’ in Latin.

*Type species.* *Samaydelphis chacaltanae* sp. nov.

*Diagnosis.* As for type species.

### *Samaydelphis chacaltanae* sp. nov.

Figures 3–9

*LSID.* urn:lsid:zoobank.org:act:70D079A9-D91E-4FC0-A15E-6F378281310D

*Derivation of name.* The species name honours Ing. César Chacaltana-Budiel, geologist, director of Environmental Geology and former head of the Paleontology Area at the Instituto Geológico Minero y Metalúrgico (INGEMMET, Peru) for his constant support of the palaeontological study of marine vertebrate assemblages of the East Pisco Basin.

*Holotype.* MUSM 566, subcomplete cranium.

*Type locality.* Cerro Colorado, East Pisco Basin, southern coast of Peru (Bianucci *et al.* 2016a, b; Di Celma *et al.* 2016; Fig. 1). Geographic coordinates: 14°19'53.9" S, 75°54'06.8" W; 480 m above sea level. This specimen was reported in the Cerro Colorado fossil map of Bianucci *et al.* (2016b) with the field number O25 and provisionally referred to as ‘Pontoporiidae n. sp.’.

*Type horizon.* Pisco Formation, P1 allomember (‘Cerro Colorado lower allomember’ in Di Celma *et al.* 2016), at 55.3 m above the contact with the underlying Chilcatay Formation (Fig. 2). This

**FIG. 2.** Stratigraphic sections (in m) of several localities of the East Pisco Basin showing the distribution in upper Miocene layers of the Pisco Formation of fossil inioids (silhouettes) including the holotype of *Samaydelphis chacaltanae* MUSM 566. All *Brachydelphis* specimens are attributed to the brevirostrine species *Brachydelphis mazeasi*, except for the one of Cerro Hueco la Zorra, only identified at the genus level. Absolute ( $^{40}\text{Ar}/^{39}\text{Ar}$  on ash layers) and biostratigraphical (diatom) age constraints of the fossil inioids are from Gariboldi *et al.* (2017) and Bosio *et al.* (2019, 2020b).  $^{40}\text{Ar}/^{39}\text{Ar}$  ages for dated ash layers (red arrows) are: CC-T1,  $9.1 \pm 0.04$  Ma; ANF-T1,  $9.31 \pm 0.01$  Ma; LB-T11,  $7.45 \pm 0.01$  Ma; LZ-T1,  $7.15 \pm 0.01$  Ma. Also reported along the sections is the position of the main marker beds (Di Celma *et al.* 2016, 2018). *Abbreviations:* Diat., diatomite; FO, first occurrence; FS, fine-grained sand; G, gravel; LO, last occurrence; MS, medium-grained sand; Silt/diat. silt, silt/diatomaceous silt; Vol. ash, volcanic ash.

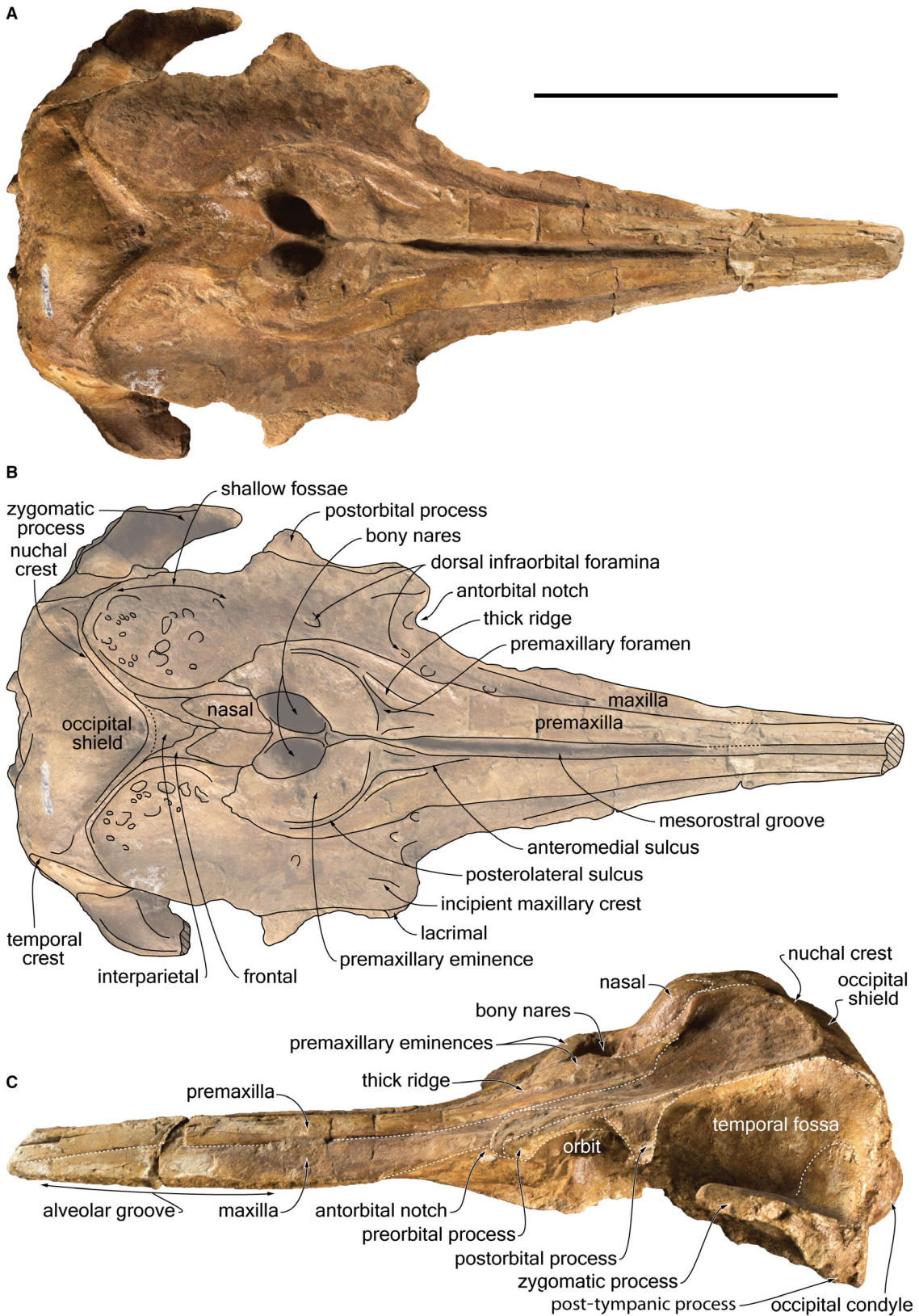


**FIG. 3.** Cranium of *Samaydelphis chacaltanae* MUSEM 566 (holotype) in: A–B, dorsal; C, left lateral view. Scale bar represents 100 mm. Colour online.

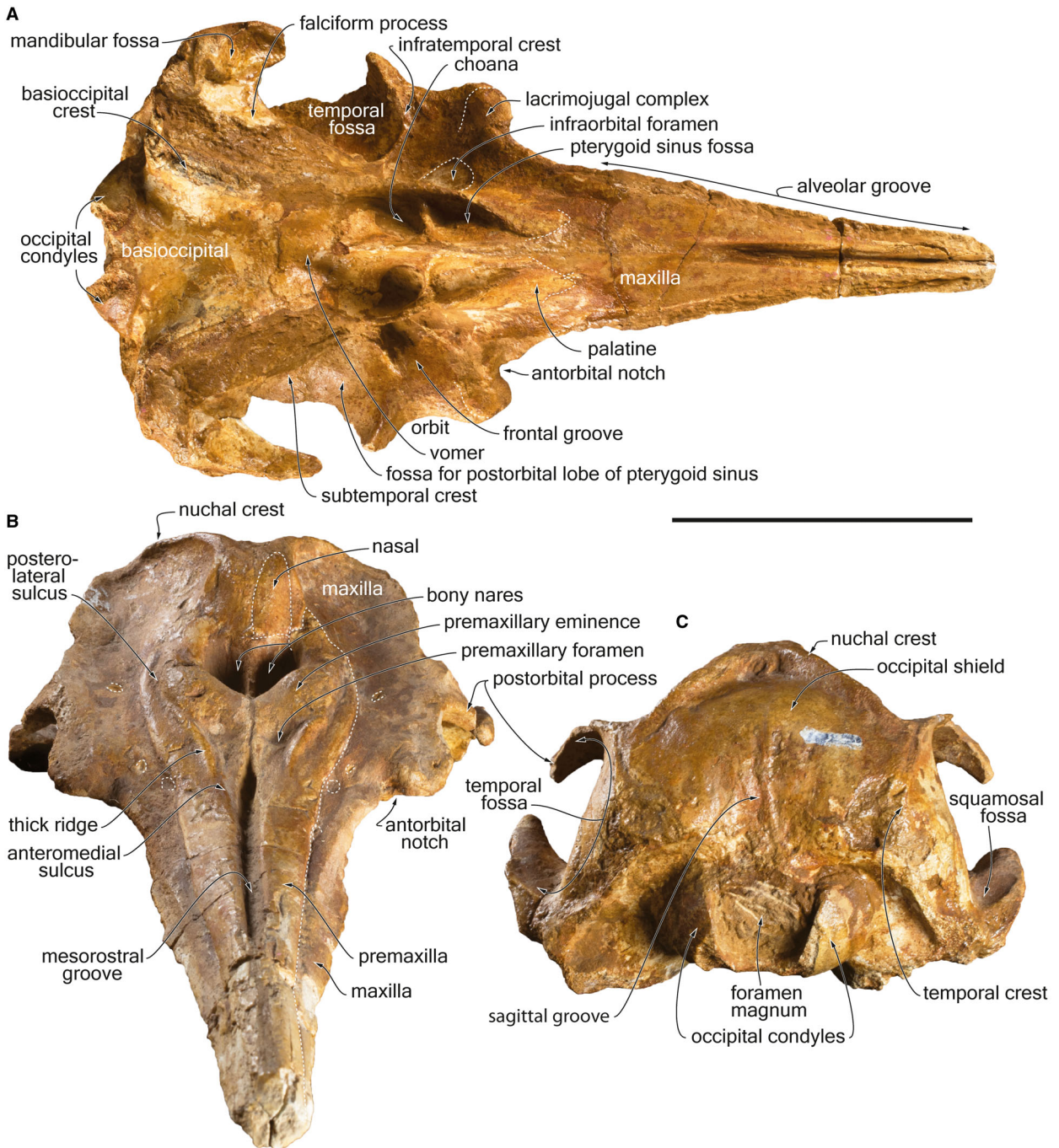


**FIG. 4.** Cranium of *Samaydelphis chacaltanae* MUSM 566 (holotype) in: A, ventral; B, anterodorsal; C, posterior view. Scale bar represents 100 mm. Colour online.

specimen is c. 25 m above a radiometrically dated volcanic ash layer (CC-T1,  $9.1 \pm 0.04$  Ma), c. 20 m above the first occurrence (FO) of *Koizumia tatsunokuchiensis* (9.0 Ma), c. 3 m above the last occurrence (LO) of *Lithodesmium reynoldsii* (8.9 Ma), and c. 10 m below the LO of *Denticulopsis praekatayamae* (8.5 Ma). As such, diatom biostratigraphy and calculated  $^{40}\text{Ar}/^{39}\text{Ar}$  ages converge to indicate an interval of deposition for the specimen-bearing strata between 8.9 and 8.5 Ma (Tortonian, early late Miocene).

*Referred specimens.* MUSM 565, subcomplete cranium, part of the axis and one thoracic vertebra. Cerro Colorado, Pisco Formation, P1 allomember, early late Miocene (9.5–8.6 Ma, Tortonian; see geological context above). Exact locality and stratigraphic horizon unknown. Approximate geographic coordinates:  $14^{\circ}20' \text{ S}$ ,  $75^{\circ}53' \text{ W}$ . MUSM 2541, partial cranium including the rostrum base, the bony nares, the vertex, and part of the supraorbital regions, a fragment of mandible with several alveoli,

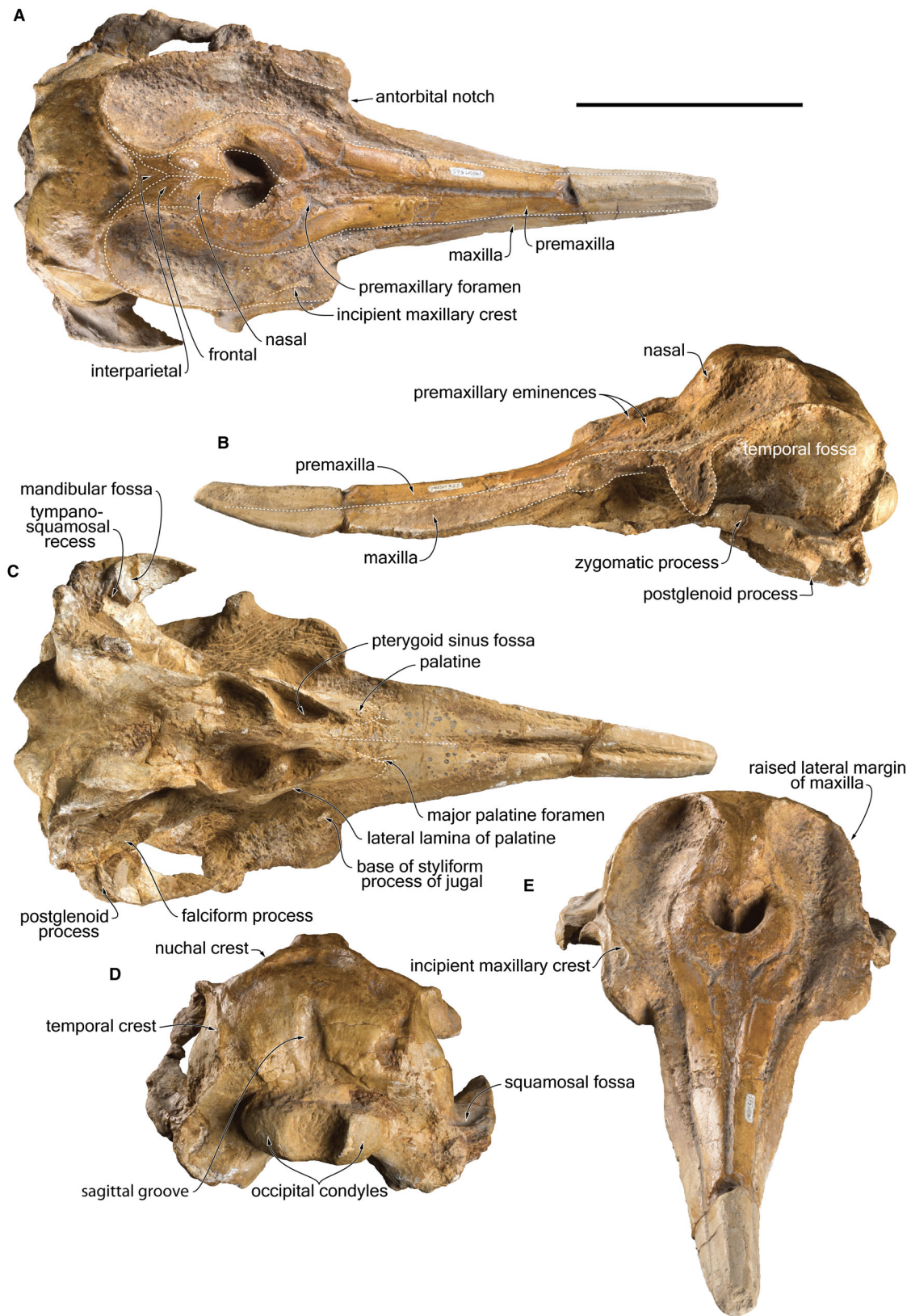


**FIG. 5.** Cranium of *Samydelphis chacaltanae* MUSM 565 in: A, dorsal; B, left lateral; C, ventral; D, posterior; E, anterodorsal view. Scale bar represents 100 mm. Colour online.



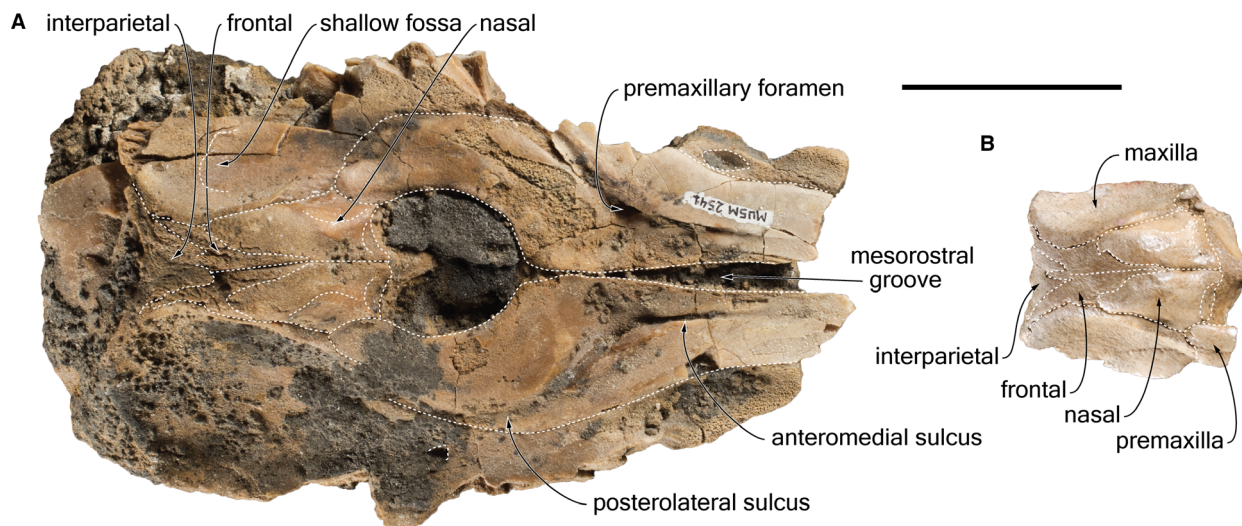


**FIG. 6.** A, partial cranium (facial region) of *Samaydelphis chacaltanae* MUSM 2541. B, vertex of *S. chacaltanae* MUSM 2512. Both in dorsal view. Scale bar represents 50 mm. Colour online.

and a few fragmented teeth. Cerro Colorado, Pisco Formation, P1 allomember, at 46.5 m above the contact with the underlying Chilcatay Formation (Fig. 2). This specimen is *c.* 12 m above the FO of *Koizumia tatsunokuchiensis* (9.0 Ma) and *c.* 5 m below the LO of *Lithodesmium reynoldsii* (8.9 Ma). As such, diatom biostratigraphy indicates an interval of deposition for the specimen-bearing strata spanning 9.0–8.9 Ma (Tortonian). Geographic coordinates: 14°22'10.5" S, 75°52'41.3" W, 582 m above sea level. MUSM 2512, fragment of cranium including the vertex. Corre Viento (Fig. 1), Pisco Formation, P1 or P2 allomember, late Miocene. Exact locality and stratigraphic horizon unknown. Approximate geographic coordinates: 14°27' S, 75°45' W. MUSM 3902, cranium missing only the left posterolateral part of the neurocranium, *c.* 1 km south of Cerro la Bruja (Fig. 1) and 16 m below the holotype of *Brujadelphis ankylorostri*, Pisco Formation, P1 allomember, early late Miocene (9.5–8.6 Ma, Tortonian; Fig. 2). Geographic coordinates: 14°33'16.8" S, 75°40'23.1" W. MUSM 3903, subcomplete cranium, Anfiteatro, Pisco Formation, P1 allomember, early late Miocene (9.5–8.6 Ma, Tortonian). The specimen has been collected *c.* 25 m above a radiometrically dated volcanic ash layer (ANF-T1, 9.31 ± 0.01 Ma; Fig. 2). Geographic coordinates: 14°32'55.41" S, 75°43'47.50" W, 582 m above sea level.

**Diagnosis.** This small size inioid (bizygomatic width between 144 and 152 mm) can be distinguished from other extinct and modern inioids by the following unique combination of morphological characters: proportionally short rostrum comprising 56–58% of the condylobasal length; no lateral groove along the premaxilla–maxilla suture on the rostrum; narrow dorsal opening of the mesorostral groove along the whole rostrum length; shallow, anterolaterally open antorbital notch; no significant dorsoventral thickening of the lacrimal; premaxillary foramen posterior to the level of the antorbital notch; dorsoventrally high and transversely thick ridge along the anteromedial border of the posterolateral sulcus; moderately dorsoventrally thickened premaxillary eminence; contact between the ascending process of

the premaxilla and the corresponding nasal; vertex of the skull significantly higher than the premaxillary eminences; nasals roughly as transversely wide as the bony nares; nasals reaching the same dorsoventral height as the frontals on the vertex; no internasal fossa; long anteromedial projection of frontals between nasals on the vertex; long anteromedial projection of interparietal between frontals on the vertex; long anteromedial projection of the occipital shield between the maxillae; ventral margin of the occipital condyles at about the same dorsoventral level as the ventral margin of the temporal fossa; broadly separated anterior apices of palatines; upper tooth count of *c.* 30 teeth per row; at least 11 post-symphyseal teeth on the mandible; no lingual heel on the crown of posterior teeth; and transverse process of the axis being posterolaterally directed. See the discussion section for a more detailed comparison with extant and extinct inioids.

### Description

**General morphology of the cranium.** With a bizygomatic width ranging from 144 to 152 mm (Table 1), *Samaydelphis chacaltanae* is a small-sized inioid, displaying a cranium that is significantly larger than in the extant *Pontoporia blainvillei*, slightly larger than in *Brachydelphis jahuayensis*, overlapping with the size interval of *Pliopontos littoralis* and *Brachydelphis mazeasi*, and smaller than in *Brujadelphis ankylorostri* and the extant *Inia geoffrensis* (Muizon 1984; Lambert & Muizon 2013; Lambert *et al.* 2017). Based on the stem delphinoid equation by Pyenson & Sponberg (2011) this range of bizygomatic widths corresponds to total body length estimates ranging between 1.48 and 1.56 m. The anterior tip of the rostrum is preserved only in MUSM 3902, where it is somewhat transversely flattened, but its anterior extent can be estimated in other rostra. The rostrum is pointed in dorsal view and proportionally short (Figs 3, 5, 7; Table 1), accounting for *c.* 56–58% of the condylobasal length (mesorostrine condition *sensu* McCurry & Pyenson 2018), with a ratio between width at rostrum base and rostrum length ranging

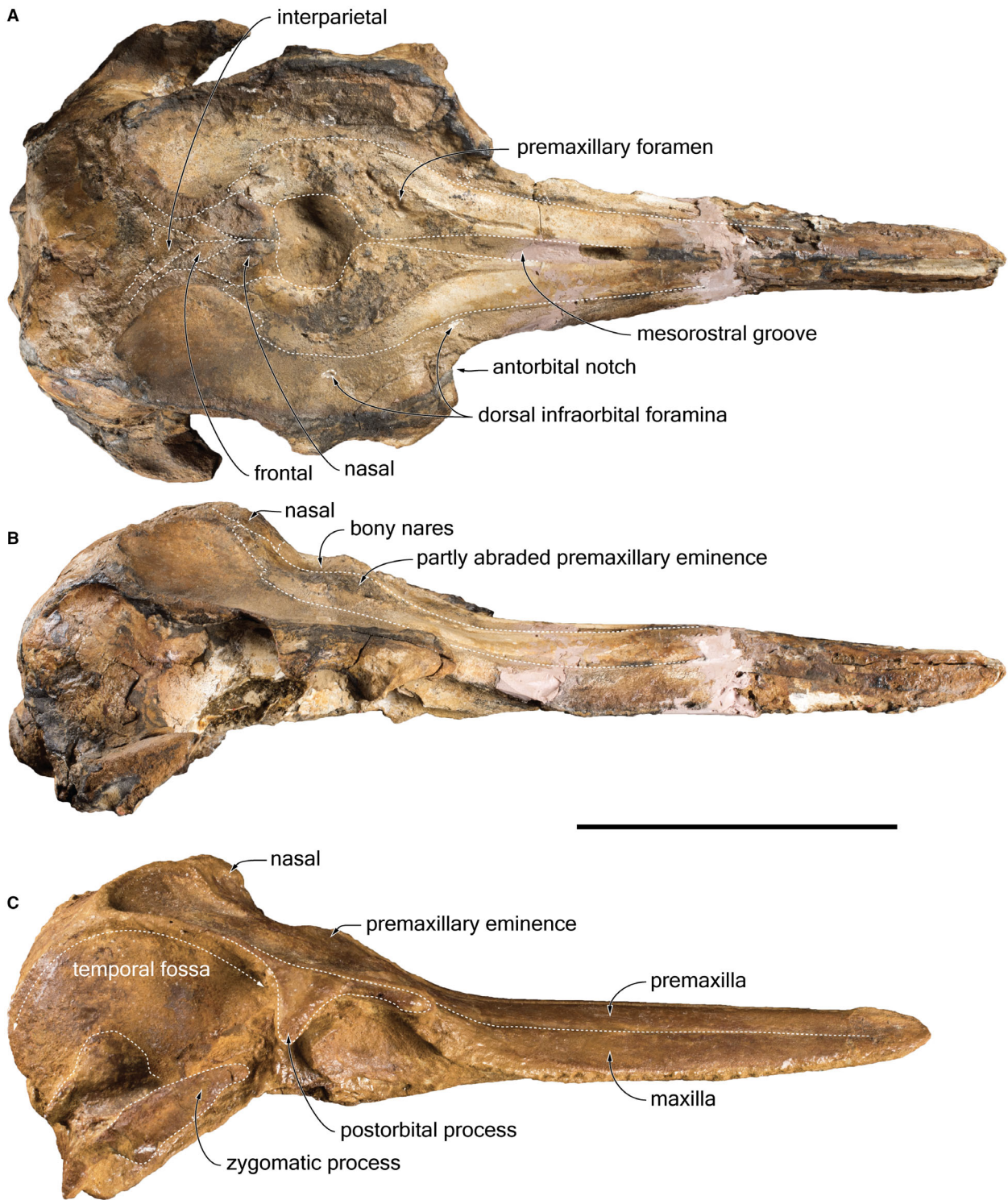


**FIG. 7.** A–B, cranium of *Samaydelphis chacaltanae* MUSM 3903 in: A, dorsal; B, right lateral view. C, cranium of *S. chacaltanae* MUSM 3902 in right lateral view. Scale bar represents 100 mm. Colour online.

from c. 0.38 to 0.42, thus being intermediate between the brevirostrine *B. mazaesi* and the longirostrine *B. jahuayensis*. Although showing a significant degree of variation in its

dimensions, the rostrum of *Pontoporia* is considerably longer (Muizon 1984, table 1). At mid-length, the cross-section of the rostrum is slightly wider than high. Differing from the other

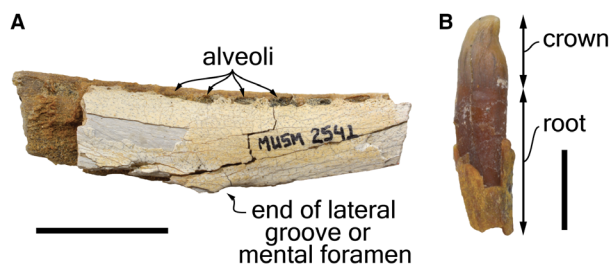


**FIG. 8.** A, fragment of right mandible of *Samaydelphis chacaltanae* MUSM 2541 in lateral view. B, detached posterior lower tooth of MUSM 2541 in mesial/distal view. Scale bars represent: 20 mm (A); 5 mm (B). Colour online.

crania that comprise the studied sample, the rostrum of MUSM 565 curves slightly anterodorsally (Fig. 5), similar to some specimens of *B. mazaesi* (Gutstein *et al.* 2009) and of a few other extinct and extant odontocetes (Bianucci *et al.* 2020). The temporal fossa is considerably anteroposteriorly longer (nearly two-fold) than the orbit, but its roof is much lower than the moderately elevated vertex (Figs 3, 5, 7). The latter is transversely narrow (minimum distance between the maxillae across the vertex lower than the width of the bony nares; Figs 3, 5–7), but not to the extent seen in *Meherrinia* (Geisler *et al.* 2012), *Pontistes* (Muizon 1984, fig. 18), and *Pontoporia*. The vertex reaches a significantly higher dorsoventral level than the dorsoventrally thick premaxillary eminences; this feature differs markedly from *Pliopontos* and *Pontoporia*, which display a much lower vertex. The facial region is moderately asymmetric, the vertex being distinctly shifted towards the left side in MUSM 565, 566, and, to a lesser degree, in MUSM 3903.

*Premaxilla.* Taking into account the incomplete apex of the rostrum in some of the studied specimens and the unfused lateral

premaxilla–maxilla suture (anterior tip of the maxilla preserved in MUSM 565 and 566), we hypothesize that the premaxilla was originally at least 15–20 mm longer anteriorly than the maxilla. In specimen MUSM 3903, three anteriormost alveoli are tentatively identified in the premaxilla. The mesorostral groove is dorsally open in the anterior portion of the rostrum (Figs 3, 5, 7). This dorsal window narrows somewhat towards the mid-part of the rostrum in MUSM 565, 566, and 3903, beyond which it broadens to reach its maximum width just anterior to the level of the antorbital notches in MUSM 566, 2541, and 3903. The right and left premaxillae contact (or almost contact) each other on the anterior margin of the anteroposteriorly short bony nares, providing this margin with a U-shape. No conspicuous dorsal exposure of the presphenoid is observed in this area. Along the rostrum, each premaxilla gradually widens towards the rostrum base, where the premaxilla is markedly wider than the maxilla in dorsal view. There is no lateral groove along the rostral premaxilla–maxilla suture, a marked difference to *Pliopontos* and *Pontoporia*. From the level of the antorbital notch, the lateral margins of the premaxillae more abruptly diverge posterolaterally, thus resulting in a distinctly laterally convex outline in the facial region. The dorsal surface of the premaxilla rises posterodorsally from the level of the antorbital notch, anterior to the premaxillary eminence. The premaxillary foramen is located posterior to the level of the antorbital notch, in a depressed triangular region that is deeper in MUSM 566 and 2541. The anteromedial sulcus is long and deep in its proximal portion, especially in MUSM 2541 and 3903, where it is shaped as a deep longitudinal slit. The posterolateral sulcus turns posterolaterally and then posteriorly, following the curve of the lateral margin of the premaxilla. Its proximal part is also deep, related to the development of a dorsoventrally high and transversely thick ridge along its anteromedial border. This ridge is conspicuous in MUSM 565, 566, 2541, and 3902, and probably present but partly worn in MUSM 3903. The posterolateral

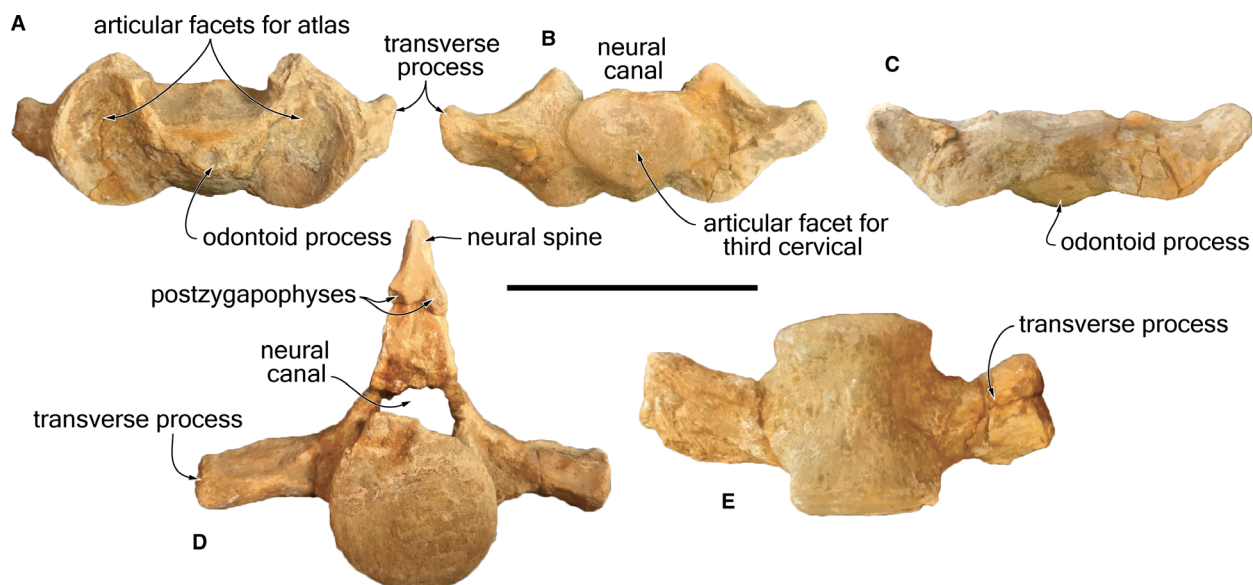


**FIG. 9.** Vertebrae of *Samaydelphis chacaltanae* MUSM 565. A–C, atlas in: A, anterior; B, posterior; C, ventral view. D–E, thoracic vertebra in: D, posterior; E, ventral view. Scale bar represents 50 mm. Colour online.

sulcus becomes shallower posterolaterally, along the premaxillary eminence, but it reaches at least the mid-length of the bony nares. The prenasal triangle is transversely concave to flat, with its medial edge rising dorsomedially in MUSM 566, 2541, and 3902. The posteromedial sulcus is barely defined, rising medially and slightly posteromedially towards the medial edge of the premaxilla. The premaxillary eminence is anteroposteriorly short (corresponding to a short distance between the premaxillary foramen and bony naris, as for example in *Brachydelphis mazeasi*) and moderately dorsoventrally thickened, although to a lesser degree than in *Scaldiporia* (Post *et al.* 2017). Its maximum height is observed along the anterior half of the bony naris. The lateral flank of the eminence is higher in MUSM 565, 566, and 3903, being nearly vertical on the right side of MUSM 565 (Figs 4, 5). Turning around the corresponding bony naris, each eminence gradually lowers and narrows posteriorly. As in other inioids, no significant asymmetry could be noted between left and right premaxillary eminences, whereas the overlying posterior part of the melon is highly asymmetric in *Pontoporia*, with a greatly reduced left branch (Frainer *et al.* 2015). From the mid-length of the bony nares, the premaxillae rise again and converge posterodorsomedially to contact the anterolateral corners of the nasals, thus being reminiscent of the condition observed in *Awadelphis*, *Brachydelphis*, and *Pontistes*. The medial margin of the ascending process of the premaxilla does not diverge laterally along the bony naris, thus not leading to a

medial exposure of the maxilla along the naris. In all the analysed specimens, the tongue-shaped posterior end of the premaxilla contacts the nasal along the anterolateral flank of the vertex on both sides of the skull, for a width of 7–10 mm (Figs 3, 5–7), a plesiomorphic condition differing markedly from *Auroracetus*, *Brujadelphis*, *Inia*, *Meherrinia*, *Pliopontos*, *Pontoporia*, *Scaldiporia*, and *Stenasodelphis*, which all lack such a contact (see Frainer *et al.* 2015, fig. 7 for a visualization of this character at different ontogenetic stages in *Pontoporia*).

*Maxilla.* In dorsal view, the maxilla is exposed lateral to the premaxilla for most of the rostrum length (Figs 3, 5, 7). Its medial margin is subvertical at the anterior end of the rostrum; posteriorly, it gradually shifts to a more dorsolateral orientation, before reducing its dorsoventral height from a level 30–40 mm anterior to the antorbital notch, as best seen in lateral view. The posteriormost portion of the lateral edge of the rostrum remains dorsoventrally thick in close proximity to the antorbital notch. In dorsal view, a slight lateral expansion of the rostrum is observed in MUSM 565, 566, and 3903, a few centimetres anterior to the antorbital notch; it is weaker than in *Parapontoporia* spp. and the recently extinct *Lipotes vexillifer* (Barnes 1985).

The antorbital processes of the maxillae are better preserved in MUSM 566, in which the left antorbital notch is deeper, related to a longer antorbital process (Fig. 3). Even there, the notch remains shallow (4.5 mm) and broadly anterolaterally

**TABLE 1.** Measurements (in mm) of the six crania of *Samaydelphis chacaltanae* described in this work.

	MUSM 566 (holotype)	MUSM 565	MUSM 2541	MUSM 2512	MUSM 3902	MUSM 3903
Condylobasal length	+295 (e310)	+310 (e320)	–	–	–	+310 (e320)
Rostrum length	+165 (e180)	+170 (e180)	–	–	165	+175 (e185)
Width of the rostrum at its base	75	68.5	–	–	e64	e70
Width of premaxillae at rostrum base	44.5	42	–	–	e42	42
Preorbital width of the skull	113	111	–	–	–	e110
Postorbital width of the skull	+132	133	–	–	–	++125
Distance between premaxillary foramina	24	21.5	24.5	–	21	22
Maximum width of bony nares	27	25	29	–	24	28
Anteroposterior length of bony nares	24.5	23.5	28	–	26	e28
Maximum width of premaxillary sac fossae	52	51	59	–	50	53
Maximum width of premaxillae	62	62	e66	–	55	62
Maximum width of nasals	23	27	27.5	26	25	27
Maximum length of nasals	32	31.5	37	29.5	–	31.5
Minimum distance between maxillae across vertex	17.5	18	15.5	11	14	15
Bizygomatic width	148	152	–	–	–	144
Maximum width of exoccipitals	118	120	–	–	–	115
Width of occipital condyles	59	59	–	–	–	57
Maximum width of foramen magnum	27.5	26.5	–	–	–	27
Height of foramen magnum	25	24	–	–	–	24
Orbit length	36.5	e37	–	–	–	–
Length of right temporal fossa	79	83	–	–	79	81
Height of right temporal fossa	53	60	–	–	57	54
Length of a segment of 8 dental alveoli (maxilla)	40	–	–	–	37	41
Length of a segment of 8 dental alveoli (mandible)	–	–	41	–	–	–

+, incomplete; –, not preserved; e, estimate.

open, differing from the deeper notch in *Brachydelphis*, *Inia*, *Isthminia*, *Pliopontos*, *Pontoporia* and *Stenasodelphis*. The right notch of MUSM 566 is nearly completely open anterolaterally, as observed in some phocoenids. The antorbital notches are, similarly, roughly directed transversely in other specimens, except for the right antorbital notch of MUSM 565 being slightly deeper and followed posteriorly by a short groove. A small dorsal infraorbital foramen is visible at the level of the antorbital notch on both sides of MUSM 566, on the right side of MUSM 3902, and on the left side of MUSM 3903 (Figs 3, 7). A few additional small foramina are probably present, in a more anterior position, along the maxilla-premaxilla suture. Posterolateral to the antorbital notch, the dorsal surface of the maxilla is thickened, marking the start of a low and generally transversely thin maxillary crest, directed posteriorly and slightly laterally towards the postorbital process, and being less developed than in *Pontoporia*. The crest is less well defined in MUSM 566. The area of the maxilla between the crest and the premaxilla is slightly depressed. From the level of the postorbital process backwards, the surface of the maxilla is transversely concave, with a slightly elevated lateral margin (less so than in *Inia*; Figs 4, 5). A tiny posterior dorsal infraorbital foramen (diameter 3–4 mm) is found in all specimens at a short distance (5–7 mm) from the premaxilla-maxilla suture and at the anteroposterior level of the postorbital process (or slightly anterior). Together with the lateral margin of the frontal, the slightly raised lateral margin of the maxilla turns posteromedially above the temporal fossa before joining the nuchal crest. The latter is higher and turns smoothly, anteromedially, towards the vertex. The maxilla reaches a level significantly posterior to the anteromedial margin of the supraoccipital, the nuchal crest drawing a deep double wave in dorsal view. The whole posterior part of the maxilla is transversely concave, more so in MUSM 565 than in other specimens. The medial margin of the maxilla rises against the vertex, with the right side being more erect (i.e. roughly vertical) in part of the specimens (MUSM 566, 2541, 3902, and 3903).

The maxillary alveoli are generally poorly preserved. In MUSM 565, the anterior alveoli display a transverse diameter of 5 mm and an interalveolar septum of 1.5–2 mm (Fig. 5). In MUSM 3902, 21 alveoli are counted along a length of 95 mm on the posterior part of the left alveolar groove, with diameters of 3–5 mm and septa shorter than 1 mm. Combining partial alveolar counts in MUSM 3902 (posteriorly) and MUSM 3903 (anteriorly), we estimate the upper tooth count at *c.* 30, in the range of *Inia* and *Lipotes*, but lower than in *Pontoporia* (Best & da Silva 1989; Brownell 1989; Chen 1989). The alveolar groove ends 20–22 mm anterior to the level of the antorbital notch in MUSM 3902 and 3903. The ventral surface of the rostrum is marked by a median trough, where the keeled ventral exposure of the vomer appears for *c.* 30 mm in MUSM 3902. Anterior to the pterygoid sinus fossae, the surface of the palate is broad and flat. Lateral to the palatine, a shallow fossa with a rounded anterior outline forms a depressed area in the rostrum base to a level 20–25 mm anterior to the antorbital notch (Figs 4, 5). Also observed in *Inia* and *Pontoporia*, this fossa probably corresponds to the area of origin for the m. pterygoideus internus (Seagars 1982). The interpretation of this fossa as housing the anterior sinus appears less likely, considering the markedly different

outline of this sinus, as reported by Fraser & Purves (1960) in *Inia*, *Lipotes* and *Pontoporia*. Best seen in MUSM 566 and 3903, the ventral infraorbital foramen is anteroposteriorly long (21 mm on the right side of MUSM 566).

*Nasal.* The nasals are prominent anterodorsally on the vertex, reaching a much higher level than the cribriform plate, the latter being lower than the posterodorsal tip of the premaxilla. In lateral view, the anterior wall of the nasal draws an angle *c.* 45° with the horizontal, sloping anteroventrolaterally, a condition reminiscent of *Meherrinia*. Each nasal is either slightly higher than the corresponding frontal (in MUSM 2541 and 3902) or roughly at the same level (in MUSM 565, 566, and 3903), thus differing from *Inia*, *Ischyrorhynchus* and *Kwanzacetus*, which have significantly lower nasals. In dorsal view, the nasals are as wide as the bony nares (a difference with *Meherrinia*, which bears narrower nasals) and wider than the frontals (to an even greater extent in MUSM 3902, in which the posterior part of the vertex is more transversely pinched; Figs 3, 5–7). The difference in transverse width between joined nasals and joined frontals on the vertex is not as great as in *Brachydelphis mazeasi*, *Brujadelphis*, *Isthminia*, *Pontistes*, *Pontoporia* and *Scaldiporia*, in which the posterior part of the vertex is even more pinched. The anterior margin of each nasal is transversely concave, with the anteromedial corner being significantly longer anteriorly than the anterolateral corner. The dorsal surface of the nasals and frontals on the vertex is roughly flat in MUSM 565, 566, 2541, 2512, and 3903, whereas the nasals bulge dorsally in MUSM 3902. In MUSM 2541, and to a lesser extent MUSM 2512, each nasal bears a well-defined facet, located anterolaterally, being slightly concave, and facing dorsolaterally. No conspicuous internasal fossa (*sensu* Muizon 1988b) is observed in any specimen, a marked difference to *Brujadelphis*, *Pontistes*, *Pontoporia*, *Scaldiporia*, and, to a lesser extent, *Auro-racetus*, *Brachydelphis*, and *Stenasodelphis*.

*Frontal.* On the vertex, each frontal sends a long and narrow projection between the nasals in MUSM 565, 566, and 3903; the projection is even longer in MUSM 2541 and MUSM 2512, equal to one-third to one-half of the anteroposterior length of the nasal (feature not visible in MUSM 3902; Figs 3, 5–7). A narrow anteromedial projection of the frontals is also observed in *Brachydelphis*, *Meherrinia*, *Pliopontos*, *Pontistes*, *Pontoporia* and *Stenasodelphis*, but it is generally shorter (except for some specimens of *Meherrinia*). The dorsal surface of the frontals is slightly depressed medially in MUSM 565, 566, and 2541. There is no frontal boss (or frontal hump; Muizon 1988b), a major difference with *Inia*, *Ischyrorhynchus*, and *Kwanzacetus*.

The preorbital process of the frontal is moderately dorsoventrally thickened, more so in MUSM 565 and 566 than in MUSM 3902 (Figs 3, 5, 7). The orbit is short compared with the temporal fossa, but less reduced than in *Inia*. The pointed postorbital process extends ventrally and slightly posterolaterally; it displays a robust base, with a triangular cross-section due to the development of the lateral part of the infratemporal crest. The latter is more poorly individualized at mid-width of the frontal in ventral view; more medially, it makes a thin and high crest for the posterior wall of the frontal groove, which is best seen in MUSM 566. At least in MUSM 566 and 3903, posterior to the frontal

groove, the medial part of the ventral surface of the frontal is deeply hollowed out, displaying a large fossa for the postorbital lobe of the pterygoid sinus that is not clearly defined laterally but that deepens somewhat dorsomedially.

The temporal fossa is only partly roofed by the frontal and maxilla; consequently, its laterally inflated medial wall is visible in dorsal view for the posterior third of its length.

*Lacrimojugal complex.* In most specimens, the base of the styli-form process of the jugal is preserved, just posterior to the antorbital notch. In ventral view of the left side of MUSM 3903, the medial suture of the jugal with the maxilla is visible, running posteriorly at some distance from the anterolateral margin of the ventral infraorbital foramen. The lacrimal–frontal suture is best seen in ventral view on the left side of MUSM 566, projecting from the anterolateral margin of the preorbital process of the frontal in a posteromedial direction, before turning medially (Fig. 4). The lacrimojugal complex is barely dorsoventrally thickened in the antorbital region (Figs 3, 5, 7), differing markedly from the dorsoventrally high complex seen in *Brachydelphis* (Muizon 1988a; Lambert & Muizon 2013).

*Palatine and pterygoid.* The palatine–maxilla suture is difficult to follow: partly visible on the right side of MUSM 566, it runs anteromedially until 33 mm anterior to the corresponding antorbital notch, beyond which it abruptly turns posteromedially. The apices of the right and left palatines are thus broadly (c. 20 mm) separated from each other, a condition similar to that observed in MUSM 565 (Figs 4, 5) and differing from the closely appressed apices of *Pliopontos* and, to a lesser extent, *Inia*. Anteromedial to the tip of the palatine, a major palatine foramen is seen on both sides of MUSM 565, 566, and 3903. The pterygoid sinus fossa reaches an anteroposterior level just anterior to the level of the antorbital notches. The anterior part of the fossa is shallow, and the fossa deepens markedly towards the anterior margin of the adjoining choana. The lateral lamina of the palatine ends at about mid-length of the choana.

There is no indication for a long lateral lamina of the pterygoid in any specimen, whereas the medial lamina is preserved in several of them. *Samaydelphis* probably differs from the living *Pontoporia* in the absence of such an extended lateral lamina of the pterygoid.

*Interparietal.* On the vertex, a small, roughly triangular bone unit is exposed, along the sagittal plane, between the supraoccipital and the frontals. From the nuchal crest it projects anteromedially, displaying either a V-shaped (MUSM 565, 566, 3902, and 3903) or W-shaped suture (MUSM 2512 and 2541) with the frontals (Figs 3, 5–7). Not being crossed by a sagittal suture in MUSM 2541, 2512, and 3903 (region not optimally preserved in MUSM 565, 566, and 3902), this bony unit does not seem to correspond to a paired bone; therefore, as in *Stenasodelphis* (see Godfrey & Barnes 2008), we interpret it as a dorsal exposure of the interparietal, which in odontocetes generally fuses with the supraoccipital early in ontogeny (Mead & Fordyce 2009). A more dorsally protruding sagittal bony element, observed in *Kwanzacetis* and several specimens of *Inia*, was similarly interpreted as part of the interparietal (Lambert *et al.* 2018).

*Supraoccipital.* As mentioned above, the occipital shield projects far anteromedially between the maxillae, as in *Meherrinia* and *Pliopontos*; characterized by a rounded anterior outline in dorsal view, the anteroposterior extent of this projection (measured from the imaginary line between the posterior ends of the maxillae to the anterior tip of the supraoccipital) ranges from 16 mm (in MUSM 565) to 23 mm (in MUSM 566; Figs 3, 5–7). As a consequence of this projection and of the highly posterodorsally inflated brain hemispheres, the dorsomedial surface of the supraoccipital is subhorizontal and separated from the nuchal crest by a clear step. The upper part of the occipital shield is transversely and dorsoventrally convex. A sagittal groove marks the lower two-thirds of its height in MUSM 565, 566, 2541, and 3903; the groove is deeper in MUSM 565, and broader and shallower in MUSM 566 and 3903. Due to the posteromedial extension of each temporal fossa, the occipital shield is moderately pinched transversely at mid-height, with the posteromedialmost part of the low temporal crest being close to the corresponding occipital condyle (Figs 4, 5). Narrow but deep dorsal condyloid fossae are observed.

*Squamosal.* The zygomatic process of the squamosal is interpreted as roughly complete on the left side of MUSM 565, on the right side of MUSM 3902, and possibly on the left side of MUSM 566 (Figs 3, 5, 7). It is long and slender, being directed anterodorsally towards the postorbital process of the frontal. Especially conspicuous in MUSM 3902 (Fig. 7), the dorsoventral tapering of the zygomatic process towards its apex is strongly reminiscent of the condition of *Pontoporia*, differing markedly from the apical dorsoventral thickening observed in *Brujadelphis*, *Inia* and *Isthminia*. The zygomatic process of *Pliopontos* and, to a greater extent, *Brachydelphis* appears, as a whole, more dorsoventrally thickened. On the left side of MUSM 565, the distance between the anterior tip of the zygomatic process and the ventral tip of the postglenoid process is 50 mm. In lateral view, its dorsal edge is slightly convex whereas its ventral edge is slightly concave. Most of its lateral surface is marked by a dorsoventrally broad longitudinal groove. The postglenoid process is short, ending ventrally as a moderately thick, transversely directed crest. The post-tympanic process is anteroposteriorly short (c. 14 mm long on the left side of MUSM 565). The floor of the squamosal fossa is slightly sigmoid along its anteroposterior axis, being convex anteriorly and concave posteriorly.

The mandibular fossa is broad and anteroventrally facing. The tympanosquamosal recess extends dorsomedial to the mandibular fossa, on the medial surface of the postglenoid process, and anterolaterally along the medial part of the ventral surface of the zygomatic process, with a lateral boundary fading away before mid-length of the process (Figs 4, 5). The falciform process (best seen in MUSM 565 and 566) is shaped as a large blade extending 22–23 mm from the medial margin of the mandibular fossa in an anteromedial direction. The foramen ovale is visible on both sides of MUSM 3903, opening laterally and slightly posteriorly, but the squamosal–alisphenoid suture could not be recognized.

*Exoccipital.* The posterior surface of the exoccipital is overhung by the posteromedially protruding temporal crest. This surface is directed laterally and dorsoventrally concave. The occipital condyles are located at a dorsoventrally low position on the

posterior wall of the neurocranium; their ventral margin is at about the ventral level of the temporal fossa (Figs 3–5, 7). However, this is not as low as in *Brachydelphis*, *Inia*, *Kwanzacetus*, *Pontoporia*, and *Scaldiporia*. The articular surfaces of the condyles face posteroventrally.

*Basioccipital*. Better preserved in MUSM 565 (Fig. 5), the basioccipital crests are slender and moderately diverge posterolaterally (making an angle c. 35° with each other), only gradually thickening distally.

*Mandible*. The 61-mm-long fragment of the right mandible of MUSM 2541 corresponds to a section just posterior to the mandibular symphysis (Fig. 8). It includes 11 complete to partly preserved alveoli, with a transverse diameter ranging from 6 to 7 mm and interalveolar septa 1–1.5 mm thick. The minimum post-symphyseal tooth count is, as in *Pliopontos*, higher than in *Inia*, *Isthminia* and *Pontoporia*. No longitudinal groove is observed along the lateral surface of this fragment, but the ventralmost part is missing and a curved region of the preserved ventral edge could correspond to the posterior end of such a groove, as seen in *Pontoporia*; alternatively, a large mental foramen may have been originally present in this region. Posterodorsal to this curved margin, a small mental foramen is observed, as, for instance, in *Brujadelpis*, *Inia*, and *Isthminia*.

*Teeth*. Only a few, partly complete single-rooted teeth of MUSM 2541 are preserved. One of them, probably a posterior lower tooth, is at least 13.8 mm long and has a conical, short crown (ratio between basal diameter and height = 0.7) and an apex curving distinctly lingually (Fig. 8). Based on its crown proportions and curvature, this tooth is interpreted as originating from the posterior part of the tooth row (see for instance *Pontoporia*'s tooth row). It lacks the typical strong lingual heel observed on the crown of posterior teeth in *Inia*. The enamel surface is slightly ornamented with numerous low ridges, which are less prominent than in *Inia* and the extinct iniid *Kwanzacetus* (Lambert *et al.* 2018).

*Vertebrae*. The epiphyses of the centrum are fused in both the axis (posterior epiphysis) and a thoracic vertebra (anterior and posterior epiphyses) of MUSM 565 (Fig. 9), suggesting that the represented individual was at least a few years old (see Galatius & Kinze 2003; Moran *et al.* 2015); however, additional vertebrae would be needed to provide more precise clues on the ontogenetic stage of this individual.

The neural arch of the axis is missing, but the rest of the bone is finely preserved. Anterior articular facets with the atlas indicate that the two first cervical vertebrae were not fused, a condition found in all other extant and extinct inioids for which this region is preserved (Van Beneden & Gervais 1880; Miller 1918; Muizon 1984; Lambert *et al.* 2017, 2018). The odontoid process is robust. The posterior epiphysis is distinctly pointed ventrally. The transverse process is robust and extends far beyond the lateral margin of the anterior articular facet for the atlas in a posterolateral direction; it is laterally longer than in *Inia* (Table 2) and differs from *Pontoporia* and *Lipotes* in not being ventrolaterally directed, being more similar to *Pliopontos*.

The preserved thoracic vertebra has a centrum that is longer than wide or high (Table 2). It has a transverse process that is at approximately the same dorsoventral height compared with the centrum as in the thoracic T10 of *Pliopontos* (Muizon 1984), but the process is proportionally markedly shorter in MUSM 565, possibly indicating a more anterior position along the thoracic segment of the vertebral column. It is worth noting that vertebrae from the mid-thoracic region have even shorter transverse processes in *Inia* and *Pontoporia* (Flower 1867; Van Beneden & Gervais 1880).

## PHYLOGENY

As in previous cladistic analyses based on an earlier version of our character–taxon matrix, inioids and other early-branching delphinidan species based on relatively fragmentary material and/or more specifically missing the ear bones tend to be highly versatile in obtained trees (Post *et al.* 2017; Lambert *et al.* 2018). For that reason, following preliminary tests we removed nine of these taxa (*Auroracetus bakerae*, *Ischyrorhynchus vanbenedeni*, *Isthminia panamensis*, *Kwanzacetus khoisani*, *Lophocetus calvertensis*, *Pithanodelphis cornutus*, *Protophocaena minima*, *Scaldiporia vandokkumi* and *Stenasodelphis russellae*) from our analysis, totalling 97 ingroup taxa. The phylogenetic relationships of the taxa listed above were individually tested and commented on in previous analyses (e.g. Geisler *et al.* 2012; Pyenson *et al.* 2015; Post *et al.* 2017; Lambert *et al.* 2017, 2018; Peredo *et al.* 2018), and we anticipate that only the discovery of new specimens with associated ear bones will allow for the relationships of all these taxa to be convincingly assessed in a single analysis. The heuristic search with a molecular constraint on

**TABLE 2.** Measurements (in mm) of the axis and one thoracic vertebra found associated with the cranium of *Samaydelphis chalcitanae* MUSM 565.

Axis	
Maximum width across anterior articular surfaces	51.1
Width across transverse processes	72.8
Width of neural arch	+20
Width of posterior articular surface	24.5
Height of posterior articular surface	18.6
Thoracic	
Anterior width of centrum	25.5
Anterior height of centrum	22.1
Posterior width of centrum	27.4
Posterior height of centrum	30.2
Length of the centrum	33.1
Width across transverse processes	74.5
Width of neural canal	14.4
Height of neural spine	+41.4

+, incomplete.

extant species applied as a backbone resulted in a single most parsimonious tree with tree length = 2021.48, consistency index = 0.16, and retention index = 0.56 (Fig. 10; for the complete tree see Lambert *et al.* 2020, file 3). In this tree *Samaydelphis chacaltanae* is recovered as sister group to *Meherrinia*, being more distantly related to a monophyletic *Brachydelphis mazeasi* + *Brachydelphis jahuyayensis*, *Pliopontos*, and the extant *Pontoporia* in the family Pontoporiidae. *Brachydelphis*, *Pliopontos*, and *Pontoporia* were similarly forming a clade in the analyses by Lambert *et al.* (2017), Post *et al.* (2017), and Lambert *et al.* (2018). As in two previous analyses *Brujadelphis* falls within Iniidae (Post *et al.* 2017; Lambert *et al.* 2018). The general topology for Iniioidea is similar to the one recovered by Lambert *et al.* (2018), differing from Post *et al.* (2017) in excluding *Atocetus* spp. from that superfamily; members of this genus fall among stem delphinidans, together with a series of taxa previously referred to the family Kentriodontidae. As in Peredo *et al.* (2018), but with a lower number of sampled taxa, Kentriodontidae is reduced to a less inclusive clade of stem delphinidans, including here *Kentriodon* and *Rudicetus*. Differing from Peredo *et al.* (2018), *Kampholophos* appears here as more closely related to *Hadrodelfhis* and *Macrokentriodon* than to *Kentriodon* and *Rudicetus*. It is worth noting that: (1) support is generally low for the recovered delphinidan clades (bootstrap values < 50, except for lipotids); and (2) the deletion of more fragmentarily known taxa considerably limits the size of the analysed sample. More complete specimens will be needed to further improve our understanding of inioid (and, more broadly, early delphinidan) phylogenetic relationships.

## DISCUSSION

Among inioids, *Samaydelphis chacaltanae* differs from *Inia* and the closely related iniids *Ischyrorhynchus* and *Kwanzacetes* (Pyenson *et al.* 2015; Lambert *et al.* 2018) in the absence of a frontal boss and the nasals reaching the same dorsal height as the frontals on the vertex; from *Inia* and *Ischyrorhynchus* in the lack of a marked ornamentation of dental enamel; and from *Inia* in the absence of a lingual heel on posterior teeth. Along with *Brujadelphis* and *Isthminia* (both recovered as iniids in previous phylogenies, as well as in the present work for *Brujadelphis*; Pyenson *et al.* 2015; Lambert *et al.* 2017, 2018) it further differs from the taxa listed above in the retention of a premaxilla–nasal contact.

*Samaydelphis* shares with *Pontoporia*, as well as with several other inioids generally identified as pontoporiids (*Auroracetes*, *Brachydelphis*, *Pliopontos*, *Pontistes*, *Protophocaena*, *Scaldiporia* and *Stenasodelphis*; Muizon 1984,

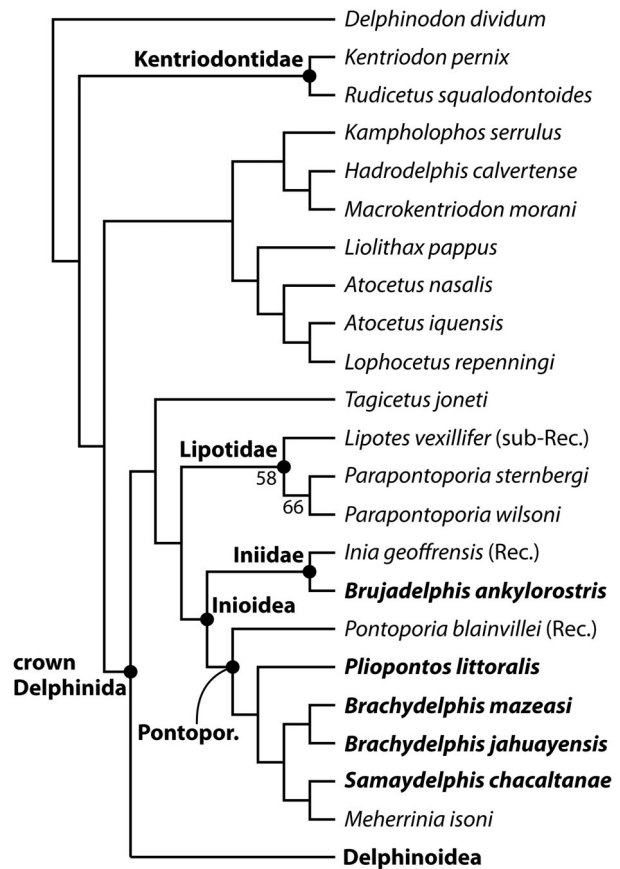


**FIG. 10.** Phylogenetic relationships of *Samaydelphis chacaltanae* with other inioids. Delphinidan part of the single most parsimonious tree resulting from the heuristic search based on a morphological character–taxon matrix, with a molecular constraint on extant cetacean species applied as a backbone (based on McGowen *et al.* 2019). The clade Delphinoidea is collapsed for clarity (for the complete tree see Lambert *et al.* 2020, file 3). Taxa in bold correspond to inioids from the late Neogene of the East Pisco Basin, Peru. *Abbreviations:* Pontopor., Pontoporiidae; Rec., Recent species; sub-Rec., recently extinct. Numbers below nodes correspond to bootstrap values (only those > 50 provided).

1988a; Lambert & Post 2005; Godfrey & Barnes 2008; Gibson & Geisler 2009; Lambert & Muizon 2013; Post *et al.* 2017), nasals that are anteroposteriorly elongated and reach the same dorsal height as the frontals on the vertex. Here again, it differs from most of the listed taxa (except *Brachydelphis*, *Pontistes*, and the more fragmentarily known *Awadelphis*) in the retention of a premaxilla–nasal contact, probably representing the plesiomorphic condition for early delphinidans. It further differs from *Pliopontos* and *Pontoporia* in the vertex reaching a considerably higher dorsoventral level than the premaxillary eminences.

The highly unusual and distinctive lowering of the vertex observed in *Pliopontos* and *Pontoporia* has recently



been investigated in relation to the soft anatomy of the forehead in the latter. In this genus, the low vertex is related to a relatively dorsoventrally low position of the bursae, soft-tissue structures involved in the production of high frequency sounds (Huggenberger *et al.* 2010). Coupled with a relatively lower encephalization quotient in *Pontoporia* (compared to *Tursiops*, for example), the low position of the bursae has been tentatively correlated to the elongation of the whole nasal complex; in turn, such an elongation of the acoustic pathway may have helped in focusing sounds (Huggenberger *et al.* 2010). The fact that earlier inioids display a higher vertex compared with *Pontoporia* supports the idea that the condition observed in the latter is a derived feature, only present in a few, later pontoporiids. Its presence in *Pliopontos littoralis* allows us to trace the origin of this major change in pontoporiid cranial topography as far back as the late Miocene (Sud-Sacaco vertebrate level, Sacaco Basin, Messinian; Muizon 1984; Ehret *et al.* 2012; Lambert & Muizon 2013). Interestingly, neonates of *Pontoporia* have premaxillary eminences that are distinctly lower than the vertex (Frainer *et al.* 2015, fig. 3), as in adults of many extinct inioids (including *Samadelphus chacaltanae*), thus differing markedly from the adult condition and suggesting that the ancestral cranial topography is retained in early ontogenetic stages of *Pontoporia*.

The combination of anteroposteriorly elongated nasals, reaching the same dorsal height as the frontals on the vertex, with a transversely pinched vertex, an extended anteromedial projection of the frontals between the nasals (reduced in part of the specimens), and an extended anteromedial projection of the supraoccipital between the maxillae has also been observed in the geologically younger *Meherrinia*, represented by nine fragmentary crania, all of which consist only of the vertex, bony nares, and part of the supraorbital processes (Geisler *et al.* 2012), from the Messinian of North Carolina. However, it differs significantly from *Samadelphus* in lacking a premaxilla–nasal contact. Tentatively referred to the family Iniidae in its initial study (Geisler *et al.* 2012), *Meherrinia* was recovered as more closely related to *Inia geoffrensis* by Pyenson *et al.* (2015) and as a stem inioid by Murakami (2016). Considering that our phylogenetic analysis supports a sister-group relationship with *Samadelphus* (Fig. 10), *Meherrinia* is here tentatively included in the family Pontoporiidae. The generally more complete inioid material from the late Miocene of the East Pisco Basin here again confirms its pivotal position for the elucidation of phylogenetic relationships for more fragmentarily known inioid taxa discovered outside Peru. Interestingly, close relationships have been proposed between *Pliopontos*, another Peruvian pontoporiid, and *Auroracetus*, a fragmentarily known member of the family from the Pliocene of North Carolina, suggesting another, possibly later

dispersal event between the south-eastern Pacific and the north-western Atlantic, before the final closure of the Isthmus of Panama (Gibson & Geisler 2009). However, in subsequent analyses *Auroracetus* was not recovered as closely related to *Pliopontos* (Geisler *et al.* 2012; Lambert *et al.* 2017), the former being a sister group of *Meherrinia* in some of the phylogenies. More complete specimens will be necessary for these two taxa to further clarify their relationships and the corresponding dispersal events. Faunal similarities between the East Pisco Basin and the east coast of North America during the late Neogene have been previously noted, for cetaceans but also for invertebrates (Muizon & DeVries 1985; Carriol *et al.* 1987).

The description of this new genus and species from the Pisco Formation further increases the diversity of inioids in the south-eastern Pacific during the late Miocene. Indeed, *Samadelphus chacaltanae* represents the fourth inioid species recorded from late Miocene levels of the Pisco Formation. Furthermore, at least three of these four species (*Brachydelphis mazeasi*, *Brujadelphis ankylorostri*, and *S. chacaltanae*) originate from the stratal package P1. These three species were coeval in a restricted interval of time spanning from  $9.31 \pm 0.01$  Ma ( $^{40}\text{Ar}/^{39}\text{Ar}$  age of the volcanic ash layer ANF-T1) to 8.5 Ma (LO of *Denticulopsis praekatayamae*) or  $8.6 \pm 0.11$  Ma ( $^{40}\text{Ar}/^{39}\text{Ar}$  age of the volcanic ash layer ZANJ-T3 from Cerros Cadenas de los Zanjones; Fig. 2). *B. mazeasi* is also found in the uppermost portion of P1 and in stratigraphically higher layers of the P2 allomember (Di Celma *et al.* 2017; Gioncada *et al.* 2018; AC, GB, OL, pers. obs.) The stratigraphically younger specimen of *Brachydelphis* that we found in the P2 allomember is a skull from Cerro Hueco la Zorra, c. 12 km north of Cerro la Bruja, for which the species could not be ascertained (either *B. mazeasi* or *B. jahuyayensis*). The age of this specimen can be constrained by combining the lithostratigraphic markers mapped by Di Celma *et al.* (2018) and radiometric ages obtained by two volcanic ash layers (Bosio *et al.* 2019, 2020b). The skull has been collected in the sediment package bounded by the P2-6 marker below and the P2-7 marker above. At Cerro la Bruja, a volcanic ash layer (LB-T11) located c. 5 m above P2-6 yielded a radiometric age of  $7.45 \pm 0.01$  Ma, whereas at Cerro Hueco la Zorra a second ash layer (LZ-T1) placed c. 25 m above P2-7 gave a radiometric age of  $7.155 \pm 0.015$  Ma. Therefore, the age of this specimen spans between 7.45 and 7.155 Ma. From a geographical point of view, *S. chacaltanae* was found together with *B. mazeasi* at Cerro Colorado (Bianucci *et al.* 2016b; this work), Corre Viento (Gioncada *et al.* 2018; this work), Cerros Cadena de los Zanjones (AC, GB, OL, pers. obs. 2013–16; this work), and also with *B. ankylorostri* south of Cerro la Bruja (Lambert *et al.* 2017; AC, GB, OL, pers. obs. 2013–16; this work).

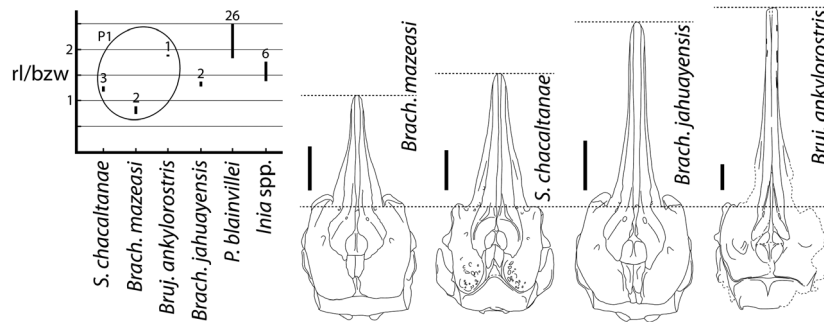


**FIG. 11.** Comparison of rostral proportions in extinct and extant inioids. Graph showing the range of the rostrum length/bizygomatic width (rl/bzw) ratio in a series of inioids from the Pisco Formation and the extant *Pontoporia blainvillei* and *Inia* spp. Numbers above ranges correspond to the number of specimens measured. Taxa that have been recorded from the stratal package P1 of the Pisco Formation are circled. Measurements taken from Flower (1867), Pilleri & Gühr (1969), Muizon (1984), Lambert & Muizon (2013) and Lambert *et al.* (2017). Schematic reconstructions of crania in dorsal view for late Miocene inioids from the Pisco Formation. Drawings of *Brachydelphis* spp. and *Brujadelphis ankylostris* modified from Lambert & Muizon (2013) and Lambert *et al.* (2017), respectively. All crania scaled at the same bizygomatic width; scale bars represent 50 mm.

In addition to size differences (with a bizygomatic width *c.* 210 mm *B. ankylostris* is significantly larger than both *B. mazeasi* and *S. chacaltanae*), these three species differ in the proportions of their rostrum (Fig. 11), ranging from the brevirostrine *B. mazeasi* to the mesorostrine *S. chacaltanae*, and the longirostrine *B. ankylostris* (categories *sensu* McCurry & Pyenson 2018). In relation to its markedly shorter rostrum, *B. mazeasi* differs in its lower tooth count (*c.* 22 vs *c.* 30 in the two other taxa), whereas the larger *B. ankylostris* displays more robust teeth on a stronger rostrum. All these differences suggest that these three sympatric species of inioids used different feeding strategies (e.g. with a greater contribution of suction in the brevirostrine *B. mazeasi*; Werth 2006; Lambert & Muizon 2013) and/or could target different prey sizes. More complete specimens, including mandibles and hyoid bones, may help to further clarify the feeding abilities of *S. chacaltanae* (e.g. Johnston & Berta 2011).

## CONCLUSION

1. Our study of a sample of six odontocete crania from the early late Miocene (Tortonian, 9.5–8.6 Ma) of four localities of the Pisco Formation in the East Pisco Basin (Peru) leads to the description of a new marine inioid genus and species, *Samaydelphis chacaltanae*.
2. *Samaydelphis chacaltanae* is a small, mesorostrine dolphin characterized by a tooth count per row of *c.* 30 teeth, a moderately elevated cranial vertex with a long anteromedial projection of both the frontals and interparietal, and the presence of a contact between premaxilla and nasal.

3. Our phylogenetic analysis recovers the new taxon as a member of the family Pontoporiidae, sister group to the North American *Meherrinia isoni* in that clade.
4. In the P1 allomember of the Pisco Formation, *S. chacaltanae* lived together with the brevirostrine pontoporiid *Brachydelphis mazeasi* and the longirostrine iniid *Brujadelphis ankylostris*. These three sympatric inioids may have differed in their feeding strategies and/or target prey sizes.
5. The discovery of more complete specimens of other known extinct inioids, as well as of ear bones of the new taxon, will help in further clarifying their phylogenetic relationships and in elucidating the early steps of the inioid radiation in marine environments.

*Acknowledgements.* We wish to warmly thank W. Aguirre for the careful preparation of specimens of the new genus and species *Samaydelphis chacaltanae* at MUSM; R. Salas-Gismondi and R. Varas-Malca for greatly facilitating our work at MUSM; S. Bruaux and O. Pauwels (IRSNB, Brussels, Belgium), S. J. Godfrey and J. R. Nance (CMM, Solomons, USA), C. Lefevre (MNHN, Paris, France), S. Farina (MSNUP, Pisa, Italy), R. Salas-Gismondi and R. Varas-Malca (MUSM, Lima, Peru), H. van der Es (NMR, Rotterdam, The Netherlands), D. J. Bohaska, J. G. Mead, C. W. Potter, and N. D. Pyenson (USNM, Washington DC, USA), and Z. Gasparini and L. H. Pomi (MLP, La Plata, Argentina) for access to collections under their care; and the reviewers S. J. Godfrey, H. Ichishima and S. Thomas for their constructive comments. This project received funding from the University of Pisa (PRA\_2017\_0032) to GB, from the Italian Ministero dell'Istruzione, dell'Università e della Ricerca (MIUR) (PRIN Project, 2012YJ5BMK EAR- 9317031) to GB, and from the National Geographic Society Committee for Research Exploration (GEFNE 177-16) to OL.

## DATA ARCHIVING STATEMENT

This published work and the nomenclatural acts it contains, have been registered in ZooBank: <http://zoobank.org/References/880E494D-01F9-4798-B1DA-8A2EF3DCDEDC>

Data for this study are available in the Dryad Digital Repository: <https://doi.org/10.5061/dryad.70rxwdbv2>

Editor. Laura Porro

## REFERENCES

- AGUIRRE-FERNÁNDEZ, G., MENNECART, B., SÁNCHEZ-VILLAGRA, M. R., SÁNCHEZ, R. and COSTEUR, L. 2017. A dolphin fossil ear bone from the northern Neotropics: insights into habitat transitions in iniid evolution. *Journal of Vertebrate Paleontology*, **37**, e1315817.
- BARNES, L. G. 1985. Fossil pontoporiid dolphins (Mammalia, Cetacea) from the Pacific Coast of North America. *Los Angeles County Museum Contributions in Science*, **363**, 1–34.
- BEST, R. C. and DA SILVA, V. M. F. 1989. Amazon river dolphin, Boto. *Inia geoffrensis* (de Blainville, 1817). 1–23. In RIDGWAY, S. H. and HARRISON, R. (eds). *Handbook of marine mammals, vol. 4: River dolphins and the larger toothed whales*. Academic Press.
- BIANUCCI, G., LAMBERT, O. and POST, K. 2010. High concentration of long-snouted beaked whales (genus *Mesapicetus*) from the Miocene of Peru. *Palaeontology*, **53**, 1077–1098.
- COLLARETA A., BOSIO, G., LANDINI, W., GARIBOLDI, K., GIONCADA, A., LAMBERT, O., MALINVERNO, E., MUIZON, C. DE, VARAS-MALCA, R., VILLA, I. M., COLETTI, G., URBINA, M. and DI CELMA, C. 2018. Taphonomy and palaeoecology of the lower Miocene marine vertebrate assemblage of Ullujaya (Chilcatay Formation, East Pisco Basin, southern Peru). *Palaeogeography, Palaeoclimatology, Palaeoecology*, **511**, 256–279.
- DI CELMA, C., COLLARETA, A., LANDINI, W., POST, K., TINELLI, C., MUIZON, C. DE, BOSIO, G., GARIBOLDI, K., GIONCADA, A., MALINVERNO, E., CANTALAMESSA, G., ALTAMIRANO-SIERRA, A., SALAS-GISMONDI, R., URBINA, M. and LAMBERT, O. 2016a. Fossil marine vertebrates of Cerro Los Quesos: distribution of cetaceans, seals, crocodiles, seabirds, sharks, and bony fish in a late Miocene locality of the Pisco Basin, Peru. *Journal of Maps*, **12**, 1037–1046.
- — LANDINI, W., POST, K., TINELLI, C., MUIZON, C. DE, GARIBOLDI, K., MALINVERNO, E., CANTALAMESSA, G., GIONCADA, A., COLLARETA, A., SALAS-GISMONDI, R., VARAS-MALCA, R., URBINA, M. and LAMBERT, O. 2016b. Distribution of fossil marine vertebrates in Cerro Colorado, the type locality of the giant raptorial sperm whale *Livyatan melvillei* (Miocene, Pisco Formation, Peru). *Journal of Maps*, **12**, 543–557.
- MUIZON, C. DE, URBINA, M. and LAMBERT, O. 2020. Extensive diversity and disparity of the early Miocene platanistoids (Cetacea, Odontoceti) in the southeastern Pacific (Chilcatay Formation, Peru). *Life*, **10**, 27.
- BOSIO, G., GIONCADA, A., MALINVERNO, E., DI CELMA, C., VILLA, I. M., CATALDI, G., GARIBOLDI, K., COLLARETA, A., URBINA, M. and BIANUCCI, G. 2019. Chemical and petrographic fingerprinting of volcanic ashes as a tool for high-resolution stratigraphy of the upper Miocene Pisco Formation (Peru). *Journal of the Geological Society*, **176**, 13–28.
- MALINVERNO, E., COLLARETA, A., DI CELMA, C., GIONCADA, A., PARENTE, M., BERRA, F., MARX, F. G., VERTINO, A. and URBINA, M. 2020a. Strontium isotope stratigraphy and the thermophilic fossil fauna from the middle Miocene of the East Pisco Basin (Peru). *Journal of South American Earth Sciences*, **97**, 102399.
- — VILLA, I. M., DI CELMA, C., GARIBOLDI, K., GIONCADA, A., BARBERINI, V., URBINA, M. and BIANUCCI, G. 2020b. Tephrochronology and chronostratigraphy of the Miocene Chilcatay and Pisco formations (East Pisco Basin, Peru). *Newsletters on Stratigraphy*, **53**, 213–247.
- BRAND, L., ESPERANTE, R., CHADWICK, A. V., POMA, O. and ALOMÍA, M. 2004. Fossil whale preservation implies high diatom accumulation rate in the Miocene–Pliocene Pisco Formation of Peru. *Geology*, **32**, 165–168.
- BRISSON, M.-J. 1762. *Regnum Animale in classes IX distributum, sine synopsis methodica*. Theodorum Haak, Paris, 296 pp.
- BROWNELL, R. L. Jr 1989. Franciscana *Pontoporia blainvillei* (Gervais and d’Orbigny, 1844). 45–67. In RIDGWAY, S. H. and HARRISON, R. (eds). *Handbook of marine mammals. Vol. 4: River dolphins and the larger toothed whales*. Academic Press.
- CARRIOL, R.-P., MUIZON, C. DE, and SECRETAN, S. 1987. Les Crustacés (Cirripedia, Crustacea) du Néogène de la Formation Pisco (Pérou). *Annales de Paléontologie*, **73**, 137–164.
- CASSENS, I., VICARIO, S., WADDELL, V. G., BALCHOWSKY, H., VAN BELLE, D., DING, W., CHEN, F., MOHAN, R. S. L., SIMOES-LOPES, P. C., BASTIDA, R., MEYER, A., STANHOPE, M. J. and MILINKOVITCH, M. C. 2000. Independent adaptation to riverine habitats allowed survival of ancient cetacean lineages. *Proceedings of the National Academy of Sciences*, **97**, 11343–11347.
- CHEN, P. 1989. Baiji *Lipotes vexillifer* Miller, 1918. 25–43. In RIDGWAY, S. H. and HARRISON, R. (eds). *Handbook of marine mammals. Vol. 4: River dolphins and the larger toothed whales*. Academic Press.
- COLLARETA, A., LANDINI, W., LAMBERT, O., POST, K., TINELLI, C., DI CELMA, C., PANETTA, D., TRIPODI, M., SALVADORI, P., CAMELLA, D., MARCHI, D., URBINA, M. and BIANUCCI, G. 2015. Piscivory in a Miocene Cetotheriidae of Peru: first record of fossilized stomach content for an extinct baleen-bearing whale. *The Science of Nature*, **102**, 1–12.
- COZZUOL, M. 2010. Fossil record and evolutionary history of Iniioidea. 193–217. In RUIZ-GARCIA, M. and SHOSTELL, J. (eds). *Biology, evolution and conservation of river dolphins within South America and Asia*. Nova Science.

- DEVRIES, T. J. 1998. Oligocene deposition and Cenozoic sequence boundaries in the Pisco Basin (Peru). *Journal of South American Earth Sciences*, **11**, 217–231.
- DEVRIES, T. and JUD, N. 2018. Lithofacies patterns and paleogeography of the Miocene Chilcatay and lower Pisco depositional sequences (East Pisco Basin, Peru). *Boletín de la Sociedad Geológica del Perú*, **8**, 124–167.
- and SCHRADER, H. 1997. Middle Miocene marine sediments in the Pisco basin (Peru). *Boletín de la Sociedad Geológica del Perú*, **87**, 1–13.
- DI CELMA, C., MALINVERNO, E., GARIBOLDI, K., GIONCADA, A., RUSTICHELLI, A., PIERANTONI, P., LANDINI, W., BOSIO, G., TINELLI, C. and BIANUCCI, G. 2016. Stratigraphic framework of the late Miocene to Pliocene Pisco Formation at Cerro Colorado (Ica Desert, Peru). *Journal of Maps*, **12**, 515–529.
- — BOSIO, G., COLLARETA, A., GARIBOLDI, K., GIONCADA, A., MOLLI, G., BASSO, D., VARAS-MALCA, R. M., PIERANTONI, P. P., VILLA, I. M., LAMBERT, O., LANDINI, W., SARTI, G., CANTALAMESSA, G., URBINA, M. and BIANUCCI, G. 2017. Sequence stratigraphy and paleontology of the upper Miocene Pisco Formation along the western side of the lower Ica Valley (Ica desert, Peru). *Rivista Italiana di Paleontologia e Stratigrafia*, **123**, 255–273.
- — — GARIBOLDI, K., COLLARETA, A., GIONCADA, A., LANDINI, W., PIERANTONI, P. P. and BIANUCCI, G. 2018. Intraformational unconformities as a record of late Miocene eustatic falls of sea level in the Pisco Formation (southern Peru). *Journal of Maps*, **14**, 607–619.
- DUNBAR, R. B., MARTY, R. C. and BAKER, P. A. 1990. Cenozoic marine sedimentation in the Sechura and Pisco basins, Peru. *Palaogeography, Palaeoclimatology, Palaeoecology*, **77**, 235–261.
- EHRET, D. J., McFADDEN, B. J., JONES, D. S., DEVRIES, T. J., FOSTER, D. A. and SALAS-GISMONDI, R. 2012. Origin of the white shark *Carcharodon* (Lamniformes: Lamnidae) based on recalibration of the Upper Neogene Pisco Formation of Peru. *Palaentology*, **55**, 1139–1153.
- FLOWER, W. H. 1867. Description of the skeleton of *Inia geoffrensis* and the skull of *Pontoporia blainvillii*, with remarks on the systematic position of these animals in the Order Cetacea. *Transactions of the Zoological Society of London*, **6**, 87–116.
- FORDYCE, R. E. and MUIZON, C. DE 2001. Evolutionary history of cetaceans: a review. 169–233. In MAZIN, J.-M. and BUFFRÉNIL, V. DE (eds). *Secondary adaptation of tetrapods to life in water*. Friedrich Pfeil.
- FRAINER, G., HUGGENBERGER, S. and MORENO, I. B. 2015. Postnatal development of franciscana's (*Pontoporia blainvillii*) biosonar relevant structures with potential implications for function, life history, and bycatch. *Marine Mammal Science*, **31**, 1193–1212.
- FRASER, F. C. and PURVES, P. E. 1960. Hearing in cetaceans: evolution of the accessory air sacs and the structure of the outer and middle ear in recent cetaceans. *Bulletin of the British Museum (Natural History), Zoology*, **7**, 1–140.
- GALATIUS, A. and KINZE, C. C. 2003. Ankylosis patterns in the postcranial skeleton and hyoid bones of the harbour porpoise (*Phocoena phocoena*) in the Baltic and North Sea. *Canadian Journal of Zoology*, **81**, 1851–1861.
- GARIBOLDI, K., BOSIO, G., MALINVERNO, E., GIONCADA, A., DI CELMA, C., VILLA, I. M., URBINA, M. and BIANUCCI, G. 2017. Biostratigraphy, geochronology and sedimentation rates of the upper Miocene Pisco Formation at two important marine vertebrate fossil-bearing sites of southern Peru. *Newsletters on Stratigraphy*, **50**, 417–444.
- GEISLER, J. H., MCGOWEN, M. R., YANG, G. and GATESY, J. 2011. A supermatrix analysis of genomic, morphological, and paleontological data for crown Cetacea. *BMC Evolutionary Biology*, **11**, 1–22.
- GODFREY, S. J. and LAMBERT, O. 2012. A new genus and species of late Miocene inioid (Cetacea: Odontoceti) from the Meherrin River, North Carolina, U.S.A. *Journal of Vertebrate Paleontology*, **32**, 198–211.
- GIBSON, M. L. and GEISLER, J. H. 2009. A new Pliocene dolphin (Cetacea: Pontoporiidae), from the Lee Creek Mine, North Carolina. *Journal of Vertebrate Paleontology*, **29**, 966–971.
- GIONCADA, A., COLLARETA, A., GARIBOLDI, K., LAMBERT, O., DI CELMA, C., BONACCORSI, E., URBINA, M. and BIANUCCI, G. 2016. Inside baleen: exceptional microstructure preservation in a late Miocene whale skeleton from Peru. *Geology*, **44**, 839–842.
- GARIBOLDI, K., COLLARETA, A., DI CELMA, C., BOSIO, G., MALINVERNO, E., LAMBERT, O., PIKE, J., URBINA, M. and BIANUCCI, G. 2018. Looking for the key to preservation of fossil marine vertebrates in the Pisco Formation of Peru: new insights from a small dolphin skeleton. *Andean Geology*, **45**, 379–398.
- GODFREY, S. J. and BARNES, L. G. 2008. A new genus and species of late Miocene pontoporiid dolphin (Cetacea: Odontoceti) from the St. Marys Formation in Maryland. *Journal of Vertebrate Paleontology*, **28**, 520–528.
- GUTSTEIN, C. S., COZZUOL, M. A., VARGAS, A. O., SUÁREZ, M. E., SCHULTZ, C. L. and RUBILAR-ROGERS, D. 2009. Patterns of skull variation of *Brachydelphis* (Cetacea, Odontoceti) from the Neogene of the southeastern Pacific. *Journal of Mammalogy*, **90**, 504–519.
- — and PYENSON N. D. 2014. The antiquity of riverine adaptations in Iniidae (Cetacea, Odontoceti) documented by a humerus from the Late Miocene of the Ituzzaingó Formation, Argentina. *The Anatomical Record*, **297**, 1096–1102.
- HAMILTON, H., CABALLERO, S., COLLINS, A. G. and BROWNELL, R. L. Jr. 2001. Evolution of river dolphins. *Proceedings of the Royal Society B*, **268**, 549–556.
- HAMPEL, A., KUKOWSKI, N., BIALAS, J., HUEBSCHER, C. and HEINBOCKEL, R. 2004. Ridge subduction at an erosive margin: the collision zone of the Nazca Ridge in southern Peru. *Journal of Geophysical Research: Solid Earth*, **109**, B02101.
- HSU, J. T. 1992. Quaternary uplift of the Peruvian coast related to the subduction of the Nazca Ridge: 13.5 to 15.6 degrees south latitude. *Quaternary International*, **15**, 87–97.
- HUGGENBERGER, S., VOGL, T. J. and OELSCHLÄGER, H. H. 2010. Epicranial complex of the La Plata

- dolphin (*Pontoporia blainvillei*): topographical and functional implications. *Marine Mammal Science*, **26**, 471–481.
- JOHNSTON, C. and BERTA, A. 2011. Comparative anatomy and evolutionary history of suction feeding in cetaceans. *Marine Mammal Science*, **27**, 493–513.
- KASUYA, T. 1973. Systematic consideration of recent toothed whales based on the morphology of tympano-periotic bone. *Scientific Reports of the Whales Research Institute*, **25**, 1–103.
- LAMBERT, O. and MUIZON, C. DE 2013. A new long-snouted species of the Miocene pontoporiid dolphin *Brachydelphis* and a review of the Mio-Pliocene marine mammal levels in the Sacaco Basin, Peru. *Journal of Vertebrate Paleontology*, **33**, 709–721.
- and POST, K. 2005. First European pontoporiid dolphins (Mammalia: Cetacea, Odontoceti), from the Miocene of Belgium and The Netherlands. *Deinsea*, **11**, 7–20.
- BIANUCCI, G. and POST, K. 2009. A new beaked whale (Odontoceti, Ziphiidae) from the middle Miocene of Peru. *Journal of Vertebrate Paleontology*, **29**, 910–922.
- — — MUIZON, C. DE, SALAS-GISMONDI, R., URBINA, M. and REUMER, J. 2010a. The giant bite of a new raptorial sperm whale from the Miocene epoch of Peru. *Nature*, **466**, 105–108.
- COLLARETA, A., LANDINI, W., POST, K., RAMASSAMY, B., DI CELMA, C., URBINA, M. and BIANUCCI, G. 2015. No deep diving: evidence of predation on epipelagic fish for a stem beaked whale from the Late Miocene of Peru. *Proceedings of the Royal Society B*, **282**, 20151530.
- BIANUCCI, G., URBINA, M. and GEISLER, J. H. 2017. A new inioid (Cetacea, Odontoceti, Delphinida) from the Miocene of Peru and the origin of modern dolphin and porpoise families. *Zoological Journal of the Linnean Society*, **179**, 919–946.
- AUCLAIR, C., CAUXEIRO, C., LOPEZ, M. and ADNET, S. 2018. A close relative of the Amazon river dolphin in marine deposits: a new Iniidae from the late Miocene of Angola. *PeerJ*, **6**, e5556.
- COLLARETA, A., BENITES-PALOMINO, A., DI CELMA, C., MUIZON, C. DE and URBINA, M. 2020. Data from: A new small, mesorostrine inioid (Cetacea, Odontoceti, Delphinida) from four upper Miocene localities in the Pisco Basin, Peru. *Dryad Digital Repository*. <https://doi.org/10.5061/dryad.70rxwdbv2>
- LANDINI, W., COLLARETA, A., PESCI, F., DI CELMA, C., URBINA, M. and BIANUCCI, G. 2017a. A secondary nursery area for the copper shark *Carcharhinus brachyurus* from the late Miocene of Peru. *Journal of South American Earth Sciences*, **78**, 164–174.
- ALTAMIRANO-SIERRA A., COLLARETA, A., DI CELMA, C., URBINA, M. and BIANUCCI, G. 2017b. The late Miocene elasmobranch assemblage from Cerro Colorado (Pisco Formation, Peru). *Journal of South American Earth Sciences*, **73**, 168–190.
- LEÓN, W., ALEMAN, A., TORRES, V., ROSELL, W. and DE LA CRUZ, O. 2008. Estratigrafía, sedimentología y evolución tectónica de la cuenca Pisco Oriental. *Boletín INGEMMET*, **27**, 1–144.
- MACHARÉ, J. and ORTLIEB, L. 1992. Plio-Quaternary vertical motions and the subduction of the Nazca Ridge, central coast of Peru. *Tectonophysics*, **205**, 97–108.
- MAROCCO, R. and MUIZON, C. DE 1988. Le Bassin Pisco, bassin cénozoïque d'avant arc de la côte du Pérou central: Analyse géodynamique de son remplissage. *Géodynamique*, **3**, 3–19.
- MARX, F. G., LAMBERT, O. and UHEN, M. D. 2016. *Cetacean paleobiology*. John Wiley & Sons, 319 pp.
- McCURRY, M. R. and PYENSON, N. D. 2018. Hyper-longirostry and kinematic disparity in extinct toothed whales. *Paleobiology*, **45**, 21–29.
- McGOWEN, M. R., TSAGKOGEOGA, G., ÁLVAREZ-CARRETERO, S., DOS REIS, M., STRUEBIG, M., DEAVILLE, R., JEPSON, P. D., JARMAN, S., POLANOWSKI, A. and MORIN, P. A. 2019. Phylogenomic resolution of the cetacean tree of life using target sequence capture. *Systematic Biology*, **69**, 479–501.
- MEAD, J. G. and FORDYCE, R. E. 2009. The therian skull: a lexicon with emphasis on the odontocetes. *Smithsonian Contributions to Zoology*, **627**, 1–248.
- MILLER, G. S. Jr 1918. A new river-dolphin from China. *Smithsonian Miscellaneous Collections*, **68**, 1–12.
- MORAN, M. M., BAJPAI, S., GEORGE, J. C., SUYDAM, R., USIP, S. and THEWISSEN, J. G. M. 2015. Intervertebral and epiphyseal fusion in the postnatal ontogeny of cetaceans and terrestrial mammals. *Journal of Mammalian Evolution*, **22**, 93–109.
- MUIZON, C. DE 1984. Les vertébrés de la Formation Pisco (Pérou). Deuxième partie: Les Odontocètes (Cetacea, Mammalia) du Pliocène inférieur de Sud-Sacaco. *Travaux de L'Institut Français D'Etudes Andines* **27**, 1–188.
- 1988a. Les vertébrés fossiles de la Formation Pisco (Pérou). Troisième partie: Les Odontocètes (Cetacea, Mammalia) du Miocène. *Travaux de L'Institut Français D'Etudes Andines*, **42**, 1–244.
- 1988b. Les relations phylogénétiques des Delphinida. *Annales de Paléontologie*, **74**, 159–227.
- and DEVRIES, T. J. 1985. Geology and paleontology of late Cenozoic marine deposits in the Sacaco area (Peru). *Geologische Rundschau*, **74**, 547–563.
- MURAKAMI, M. 2016. A new extinct inioid (Cetacea, Odontoceti) from the Upper Miocene Senhata Formation, Chiba, central Japan: the first record of Inioida from the North Pacific Ocean. *Paleontological Research*, **20**, 207–225.
- PARHAM, J. F. and PYENSON, N. D. 2010. New sea turtle from the Miocene of Peru and the iterative evolution of feeding ecomorphologies since the Cretaceous. *Journal of Paleontology*, **84**, 231–247.
- PEREDO, C. M., UHEN, M. D. and NELSON, M. D. 2018. A new kentriodontid (Cetacea: Odontoceti) from the early Miocene Astoria Formation and a revision of the stem delphinidan family Kentriodontidae. *Journal of Vertebrate Paleontology*, **38**, e1411357.
- PILGER, R. H. Jr. 1981. Plate reconstructions, aseismic ridges, and low-angle subduction beneath the Andes. *Geological Society of America Bulletin*, **92**, 448–456.

- PILLERI, G. and GIHR, M. 1969. Zur anatomie und pathologie von *Inia geoffrensis* de Blainville 1817 (Cetacea, Susuidae) aus dem Beni, Bolivien. *Investigations on Cetacea*, **1**, 94–106.
- POST, K., LOUWYE, S. and LAMBERT, O. 2017. *Scaldiporia vandokkumi*, a new pontoporiid (Mammalia, Cetacea, Odontoceti) from the Late Miocene to earliest Pliocene of the Westerschelde estuary (The Netherlands). *PeerJ*, **5**, e3991.
- PYENSON, N. D. and HOCH, E. 2007. Tortonian pontoporiid odontocetes from the Eastern North Sea. *Journal of Vertebrate Paleontology*, **27**, 757–762.
- and SPONBERG, S. N. 2011. Reconstructing body size in extinct crown Cetacea (Neoceti) using allometry, phylogenetic methods and tests from the fossil record. *Journal of Mammalian Evolution*, **18**, 269–288.
- VÉLEZ-JUARBE, J., GUTSTEIN, C. S., LITTLE, H., VIGIL, D. and O'DEA, A. 2015. *Isthminia panamensis*, a new fossil inioid (Mammalia, Cetacea) from the Chagres Formation of Panama and the evolution of 'river dolphins' in the Americas. *PeerJ*, **3**, e1227.
- RAMASSAMY, B., LAMBERT, O., COLLARETA, A., URBINA, M. and BIANUCCI, G. 2018. Description of the skeleton of the fossil beaked whale *Messapicetus gregarius*: searching potential proxies for deep-diving abilities. *Fossil Record*, **21**, 11–32.
- SEAGARS, D. J. 1982. Jaw structure and functional mechanics of six delphinids (Cetacea: Odontoceti). Unpublished Master's thesis, San Diego State University, 179 pp.
- STUCCHI, M., VARAS-MALCA, R. M. and URBINA-SCHMITT, M. 2016. New Miocene sulid birds from Peru and considerations on their Neogene fossil record in the Eastern Pacific Ocean. *Acta Palaeontologica Polonica*, **61**, 417–427.
- SUESS, E., VON HUENE, R. and EMEIS, K. 1988. Introduction, objectives, and principal results, Leg 112, Peru continental margin. *Proceedings of ODP, Initial Reports*, **112**, 5–23.
- SWOFFORD, D. L. 2003. PAUP\*. Phylogenetic analysis using parsimony (\*and other methods). Version 4. Sinauer Associates, Sunderland, MA.
- THORNBURG, T. M. and KULM, L. D. 1981. Sedimentary basins of the Peru continental margin: structure, stratigraphy, and Cenozoic tectonics from 6°S to 16°S latitude. 393–422. In KULM, L. D., DYMOND, J., DASCH, E. J. and HUSONG, D. M. (eds). *Nazca plate: Crustal formation and Andean convergence*. Geological Society of America Memoir, **154**.
- TRAVIS, R. B., GONZALES, G. and PARDO, A. 1976. Hydrocarbon potential of Coastal Basins of Peru. *AAPG Memoir*, **25**, 331–338.
- UHEN, M. D. 2008. New protocetid whales from Alabama and Mississippi, and a new cetacean clade, Pelagiceti. *Journal of Vertebrate Paleontology*, **28**, 589–593.
- VAN BENEDEN, P.-J. and GERVAIS, P. 1880. *Ostéographie des cétacés vivants et fossiles*. Arthus Bertrand, Paris, 634 pp.
- WERTH, A. J. 2006. Mandibular and dental variation and the evolution of suction feeding in Odontoceti. *Journal of Mammalogy*, **87**, 579–588.